# X-RAY PHASE CONTRAST AND MULTIPLE - ANGLE STEREOMETRY FOR 3-D RECONSTRUCTION: FATIGUE CRACKS IN ALUMINUM

---

Konstantin Ignatiev

*Materials Science and Engineering Dept.*

*Georgia Institute of Technology*

Georgia Institute of Technology

# Outline

- Background
- X-ray Phase Contrast Imaging
- Stereometry
- Results
- Conclusion

# Background

# Al-Li alloys

- High specific strength
- Alloy AA2090 - abnormally low fatigue crack propagation rate due to roughness induced crack closure

# Fatigue crack closure

**Premature contact during unloading (prolonged contact during loading) thought responsible for up to 10X decrease in fatigue crack growth rate !!!**

## Closure mechanisms

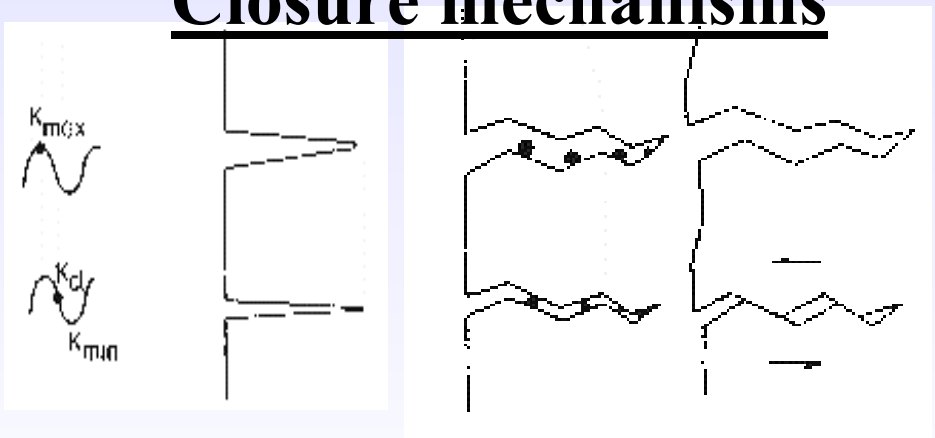


**none** **particle** **roughness**

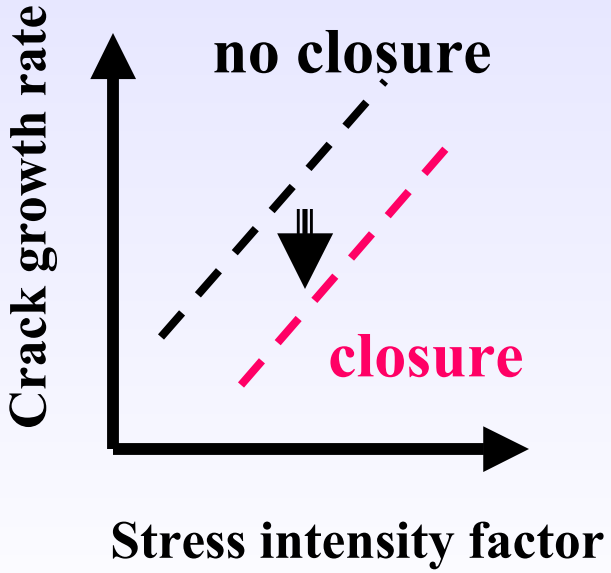

# Load deflection curve for a small compact tension sample

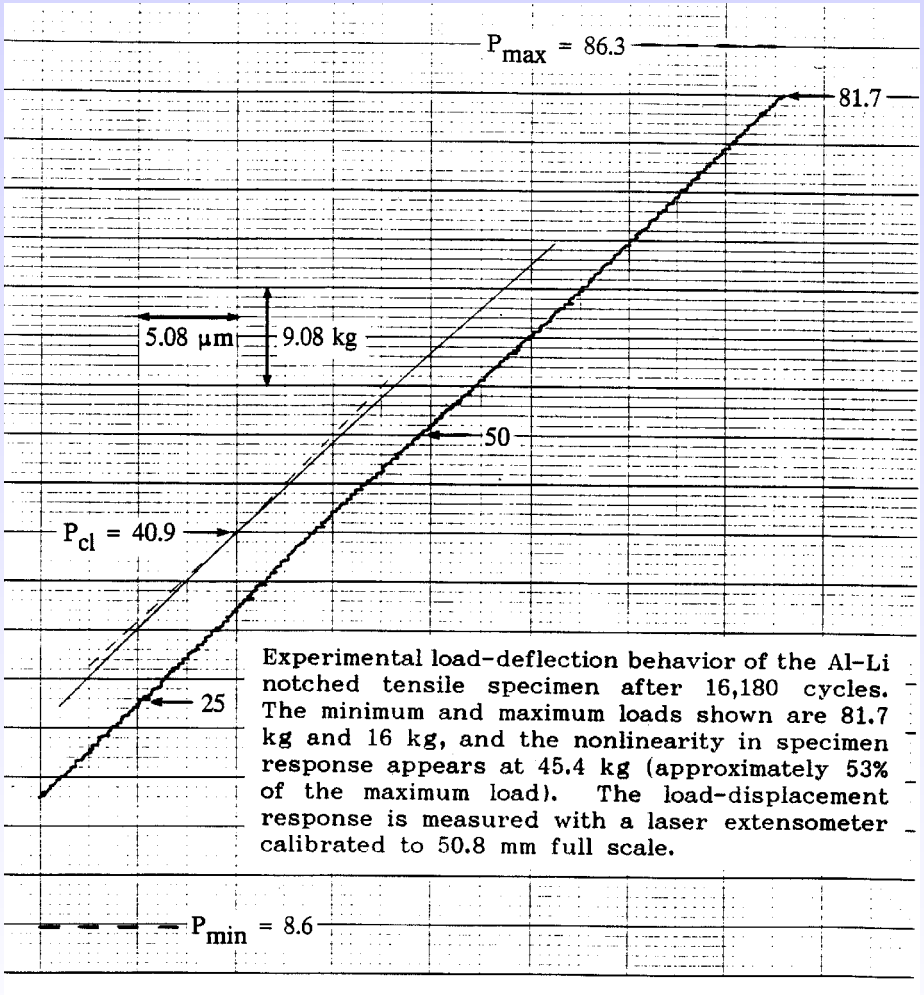


Experimental load-deflection behavior of the Al-Li notched tensile specimen after 16,180 cycles. The minimum and maximum loads shown are 81.7 kg and 16 kg, and the nonlinearity in specimen response appears at 45.4 kg (approximately 53% of the maximum load). The load-displacement response is measured with a laser extensometer calibrated to 50.8 mm full scale.

# Aluminum alloy AA2090

**Chemical composition (in weight percent)**

| Li | Cu | Mg | Zn | Zr | Mn | Cr | Ti | Fe | Si | Al |
|---|---|---|---|---|---|---|---|---|---|---|
| 1.9-2.6 | 2.4-3.0 | 0.25 max | - | 0.08-0.15 | 0.05 max | - | 0.15 max | 0.12 max | 0.1 max | bal. |

Grain dimensions (at the center of plate), μm

| | L | T | S |
|---|---|---|---|
| Al-Li 2090 T8E41 | 2500 | 500 | 50 |

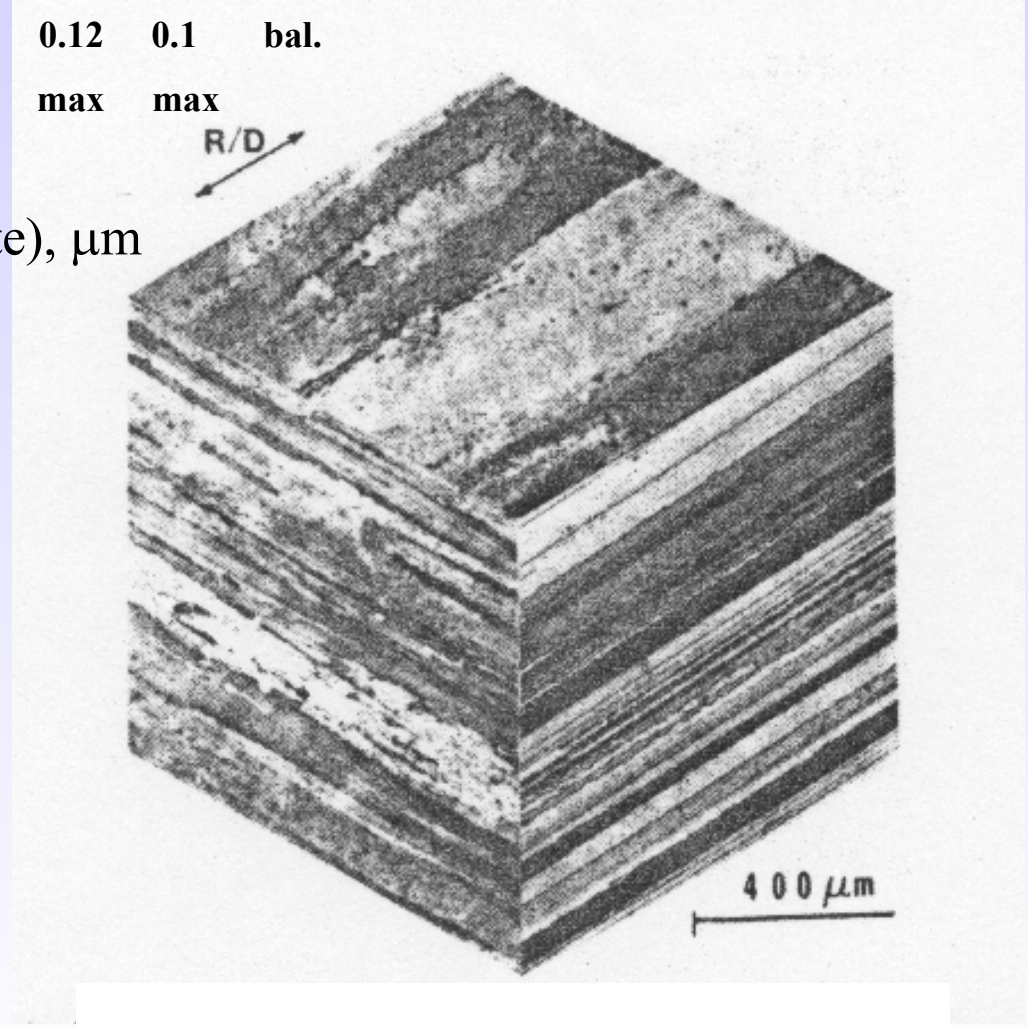


*W.Yu, R.O.Ritchie.*
*Journal of Engineering Materials and Technology*
*1987, Vol.109,p.81*

Coherent and shearable δ' ($Al_3Li$) precipitates promote planar slip crack behavior

# Fatigue cracks in Al-Li

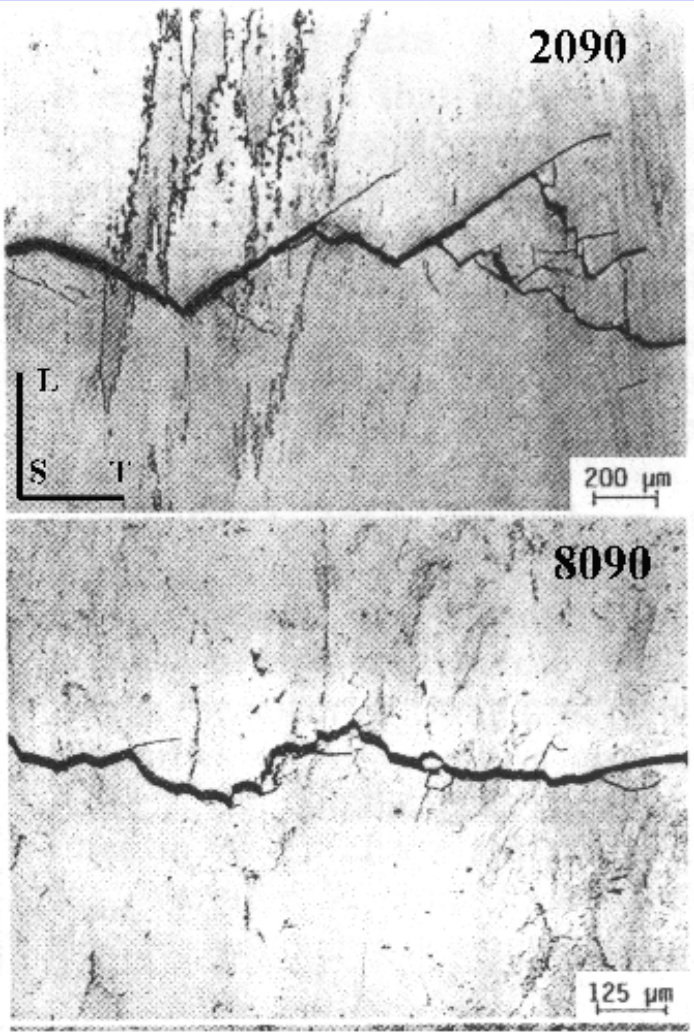


L-T orientation, R=0.1, t/2 location

K.T.V.Rao, R.O.Ritchie. International Materials Reviews 1992. vol.37. 4

Optical and SEM studies revealed that the highly non-planar jagged crack is responsible for the crack path closure in L-T oriented compact tension samples of AA 2090.

Previous microdiffraction investigations showed that this is due to a specific mesostructure: regions of AA 2090 alloy consist of near single crystal material containing 5 to 10 pancake-shaped grains.

Passage of the crack through these volumes forms the large asperities in AA 2090.

Other Al-Li alloys, which have more planar crack paths and which exhibit normal fatigue crack growth rates, do not have this type of mesostructure.

# X-ray methods are best-suited for studying crack closure

- Advantages (as opposed to):

  - Non-destructive (serial sectioning). Can use in-situ measurements

  - Gives information about the optically opaque volume, not just the surface (Optical and electron microscopy)

<u>Crack propagation, opening are 3-D processes</u>

X-ray absorption microtomography has been previously used for crack closure study in Al-Li alloy, however it has limitations due to the shape of the sample

# 3-D representation of opening vs. position for different loads

## Circumferentially notched cylindrical sample of Al

**Mesh: 3D position of crack**

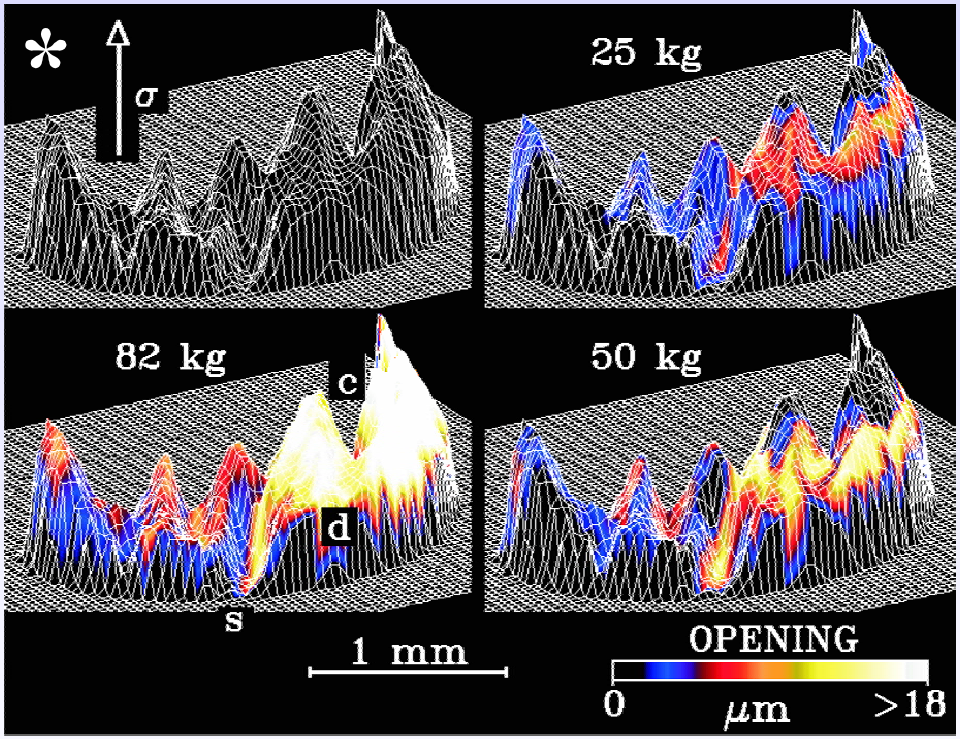


**Color: crack opening**

*Guvenilir, Breunig, Kinney, Stock (1997) Acta mater 45,1977-1987.

**View: sample exterior from crack initiation point**

Compact tension geometry is widely used for fatigue testing, large database exists, much more straightforward fracture mechanics calculations

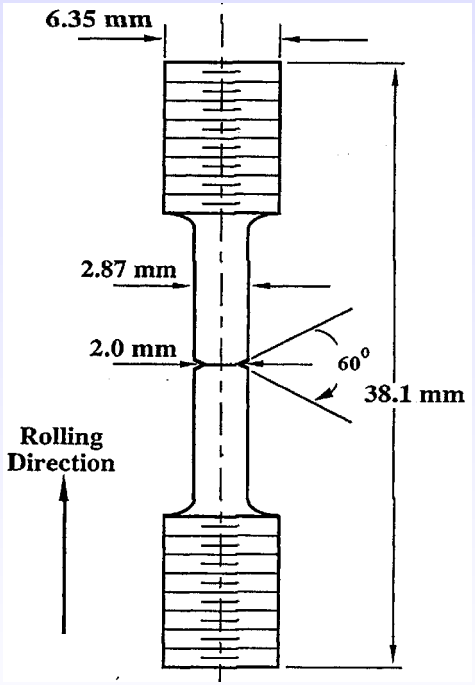


Notched tensile

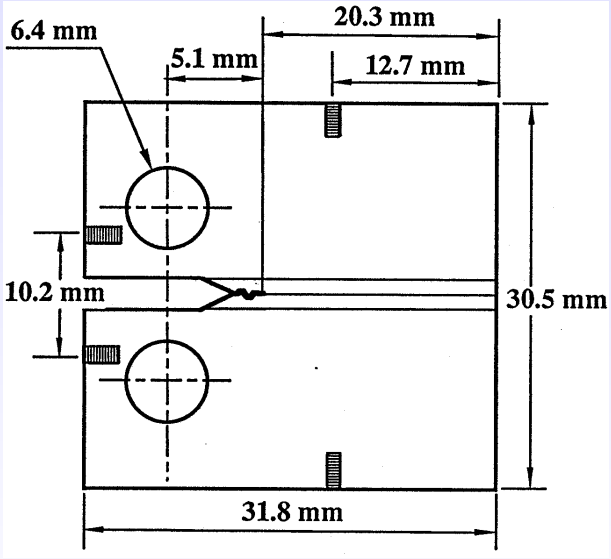


Compact tension

# Limitation of computed tomography methods with respect to the study of high aspect ratio samples

Fracture mechanics dictates sample geometries, which limit the crack opening sensitivity that can be obtained with microtomography

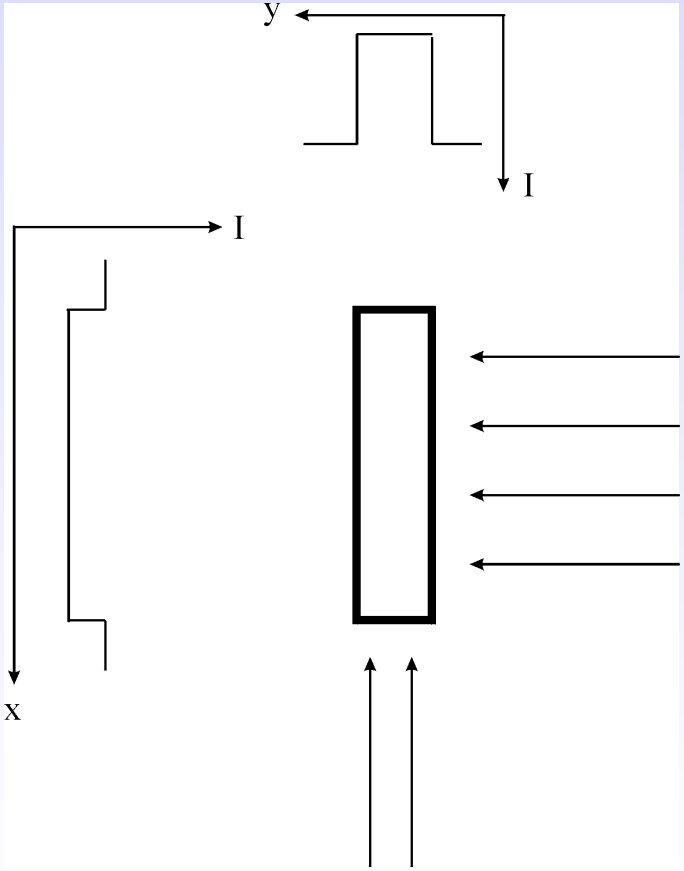


- Fixed number of detector elements means that for large field of view, voxel size will be large, sensitivity to crack openings will be decreased
- Very long x-ray paths through the sample in certain orientations limit the sensitivity

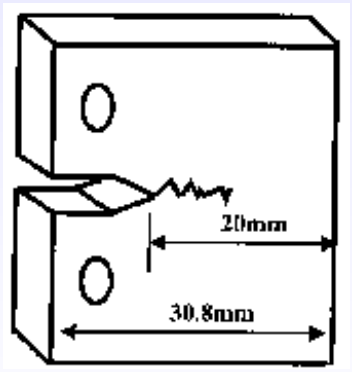


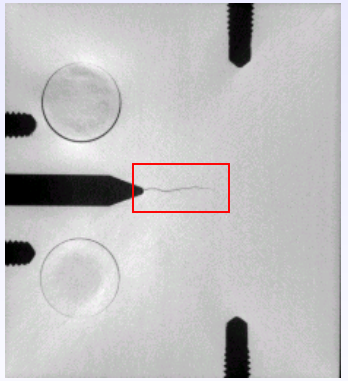

# Compact tension specimen slices obtained with microtomography

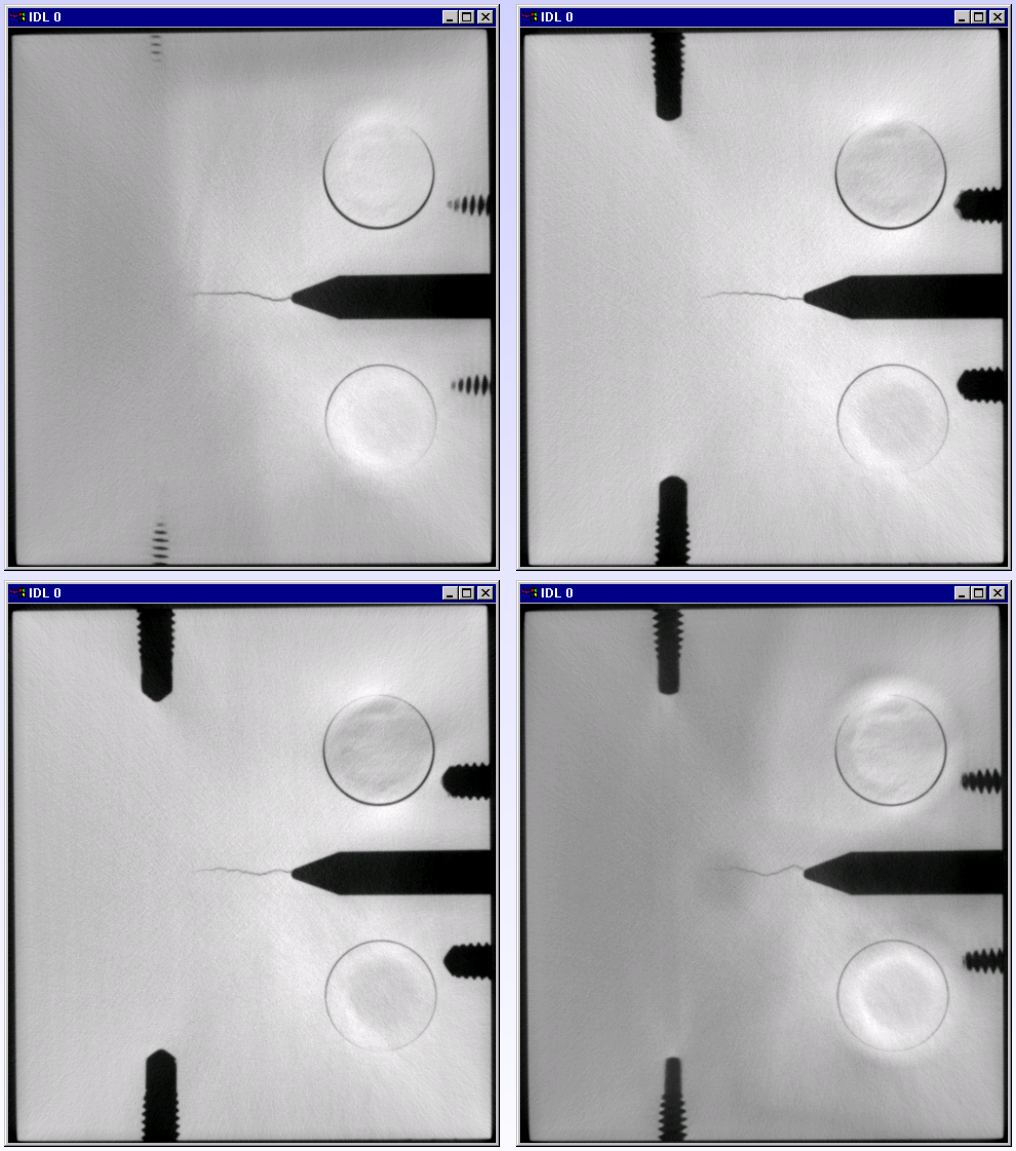


On the left, reconstructed microtomography slices of compact tension specimen CT43M are shown (every 20$^{th}$ slice).

On the bottom – magnified area near the notch.

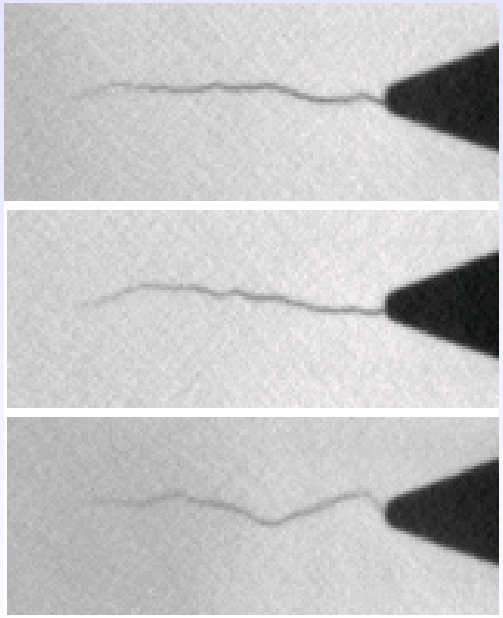

# Possible solutions

- Cut out area of the sample near the tip of the crack
- Use limited-angle CT

X-ray phase contrast imaging can be used to overcome limitations on the sample size and shape without degrading resolution or sensitivity

# X-ray phase contrast

- **In most materials the index of refraction for x-rays differs slightly from 1 and depends on electron density in a way that is different from absorption.**

- **If the x-ray wavefield propagating through a uniform solid encounters volumes with different refractive indices, the wavefront is distorted …edge enhancement, multiple fringes. Changes which are too small to be seen with absorption as the source of contrast are readily seen with phase (provided that the incident beam has the proper characteristics).**

# Schematics of several X-ray phase contrast imaging methods

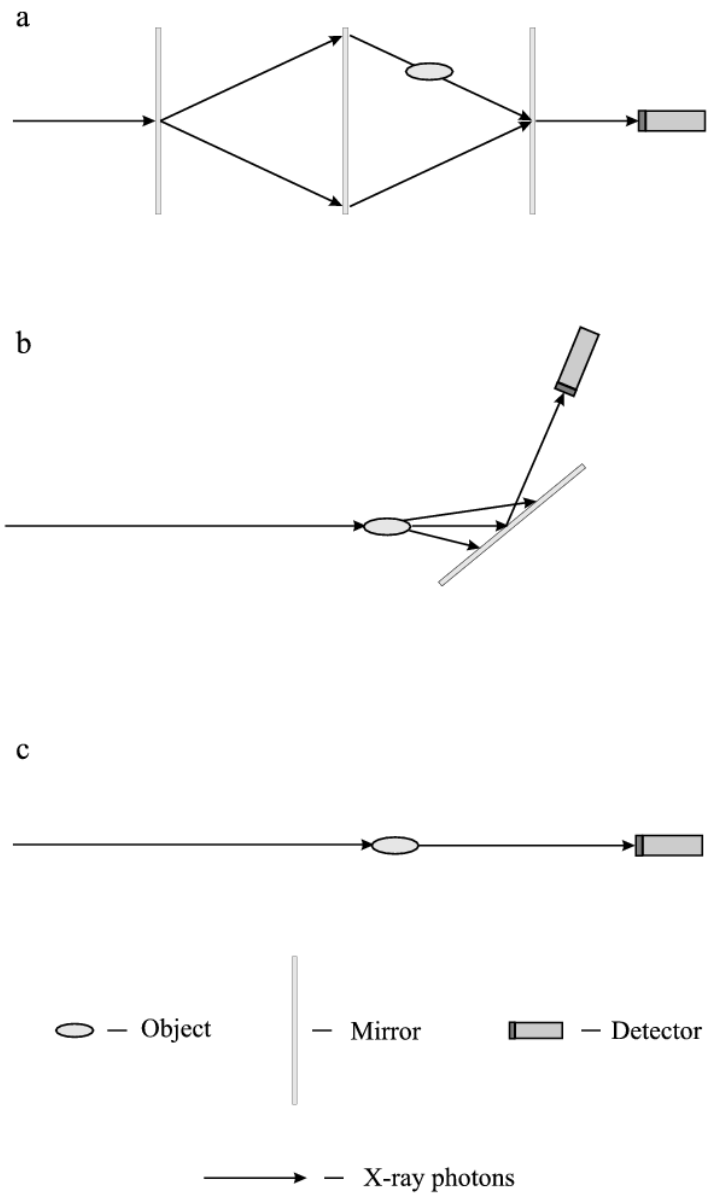


Interferometer method

Diffraction-enhanced method

Propagation method

# X-ray Phase Propagation Method

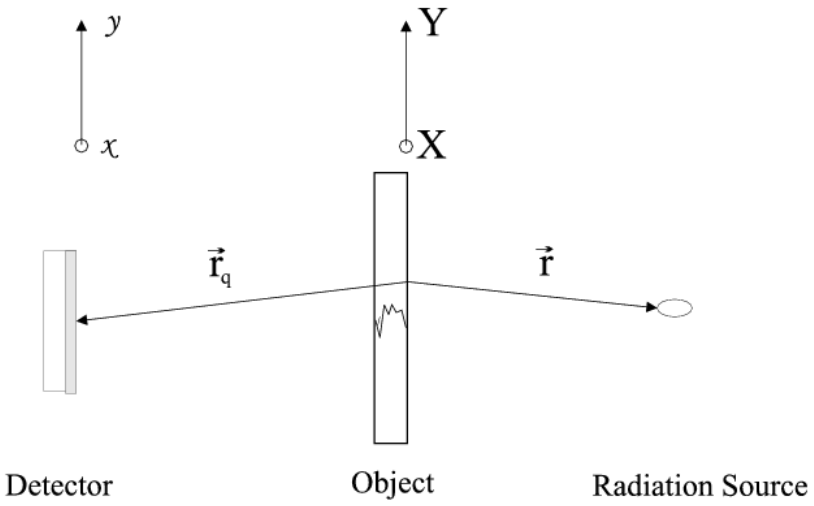


$$n = 1 - \delta + i\beta$$

$\delta \sim 10^{-7}$ - phase contrast

$\beta \sim 10^{-10}$ - absorption

$$\beta = \frac{\mu\lambda}{4\pi}$$

$$\Psi = Q * P,$$

$$Q(X,Y) = A(X,Y)\ \exp\left[i\varphi(X,Y)\right]$$

$$A(X,Y) = \exp\left[-\frac{1}{2}\int \mu(X,Y,Z)\,dZ\right]$$

$$\varphi(X,Y) = -\frac{2\pi}{\lambda}\int \delta(X,Y,Z)\,dZ$$

Change in the phase of the wave over distance transforms into the change of the intensity distribution of the wave, that can be detected (lense-less wavefront reconstruction).

# Comparison of absorption and phase contrast images

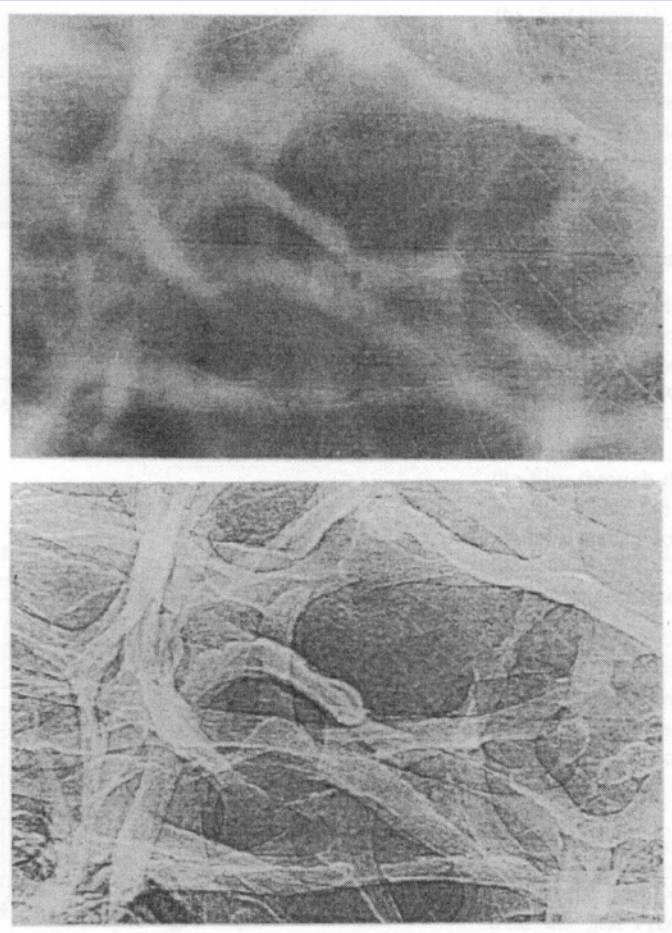

From P. Cloetens, R. Barrett, J. Baruchel et al. *Journal of Physics D-Applied Physics* 29 (1):133-146, 1996.

# Change of phase contrast pattern with increasing sample-detector distance

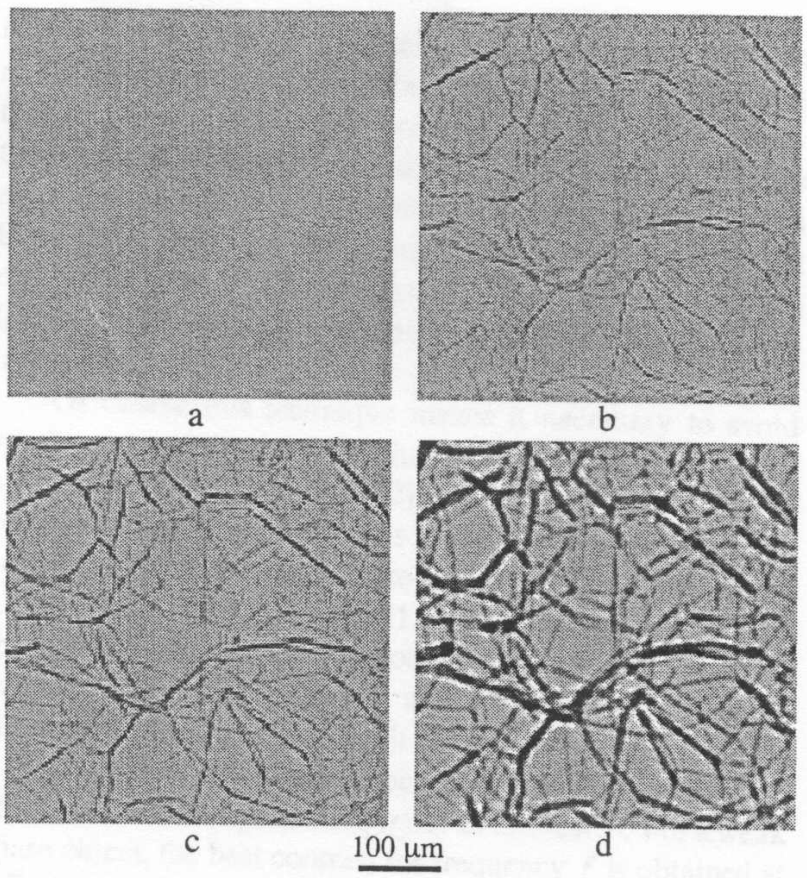


**Figure 1.** Phase-sensitive radiographs of a 1 mm thick piece of polystyrene foam, with the film at various distances $d$ from the specimen. X-ray wavelength $\lambda = 0.69$ Å. (*a*) $d = 0.01$ m; (*b*) $d = 0.12$ m; (*c*) $d = 0.22$ m; (*d*) $d = 0.91$ m. The contrast and the width of the interference fringes increase throughout the series.

From P. Cloetens, W. Ludwig, J. Baruchel et al. *Journal of Physics D-Applied Physics* 32 (10A):A145-A151, 1999.

# Cracks are good objects for phase contrast imaging!

- Sharp change in index of refraction between air and aluminum
- Contrast forms only at certain points of the crack (edge detection)
- Can see the crack instantly (no reconstruction needed)

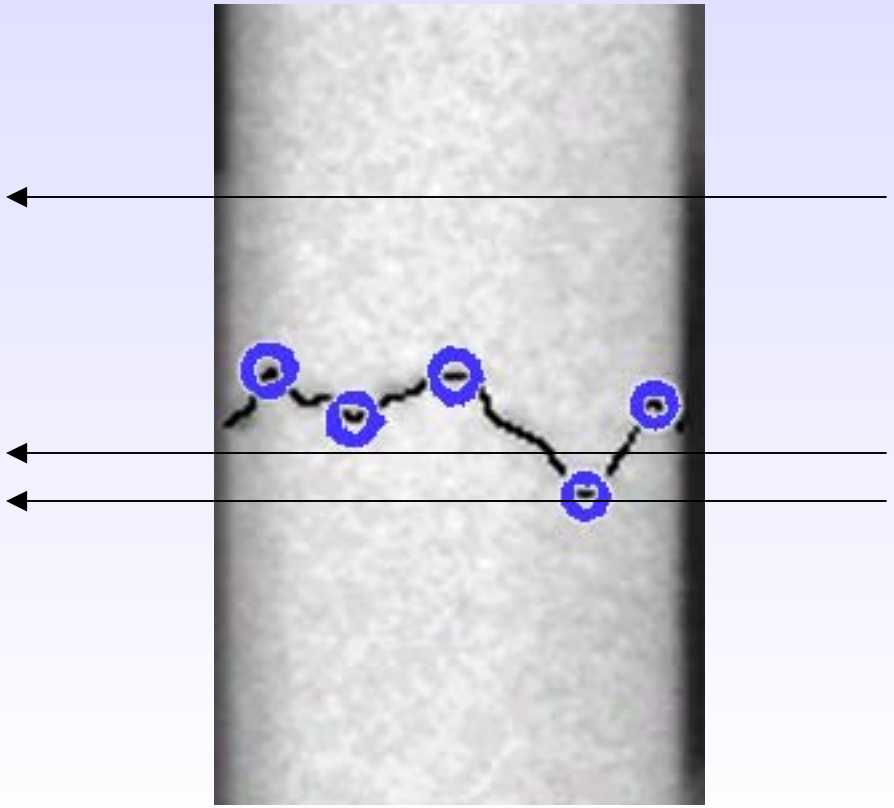

1

2

3

Path 1 – No contrast

Path 2 – No contrast

Path 3 - Contrast

Blue circles represent sharp change in crack surface geometry.

# Phase contrast images of rotation about compact tension sample Y axis

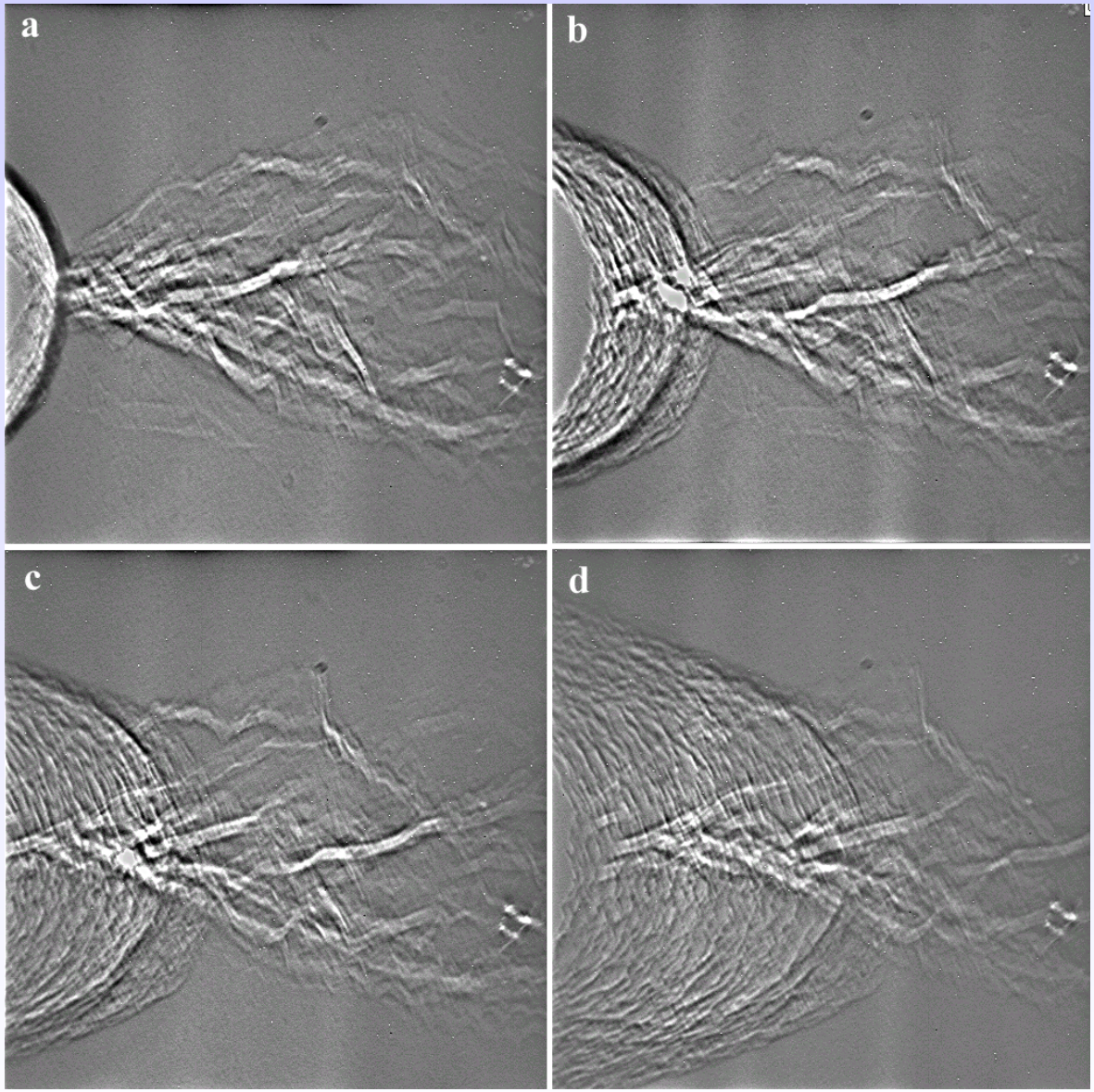


5 degree increment

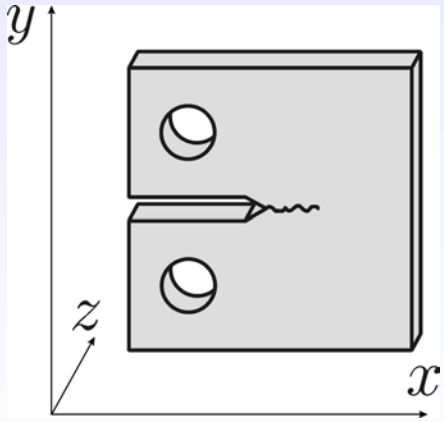

# Phase contrast images of rotation about compact tension sample Y axis

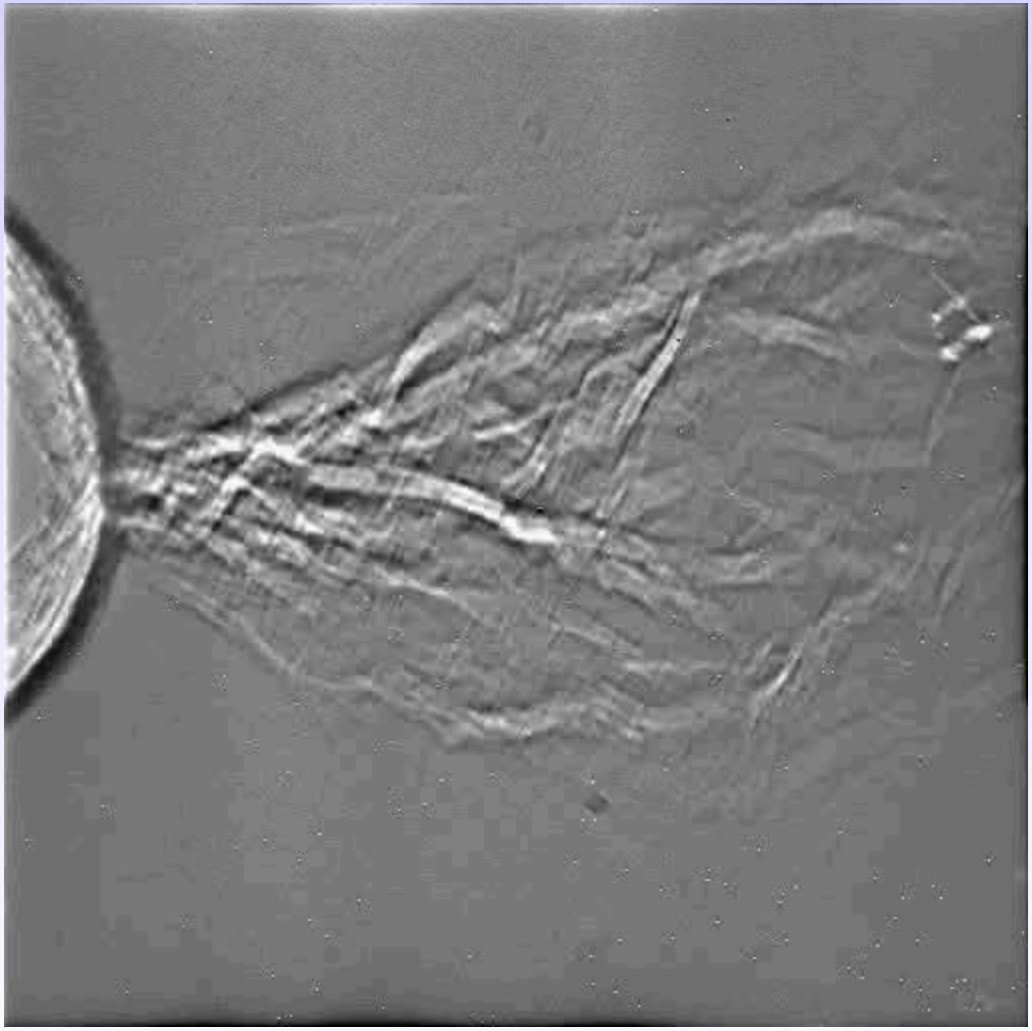

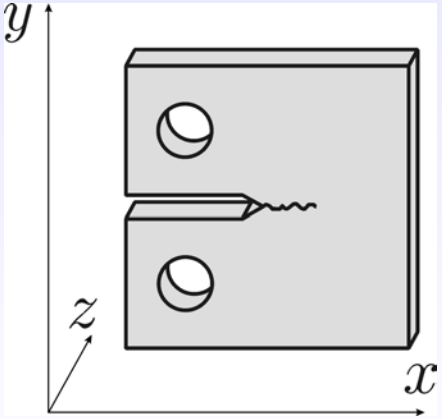

# Stereo Reconstruction

# Stereometry

## Projection geometry

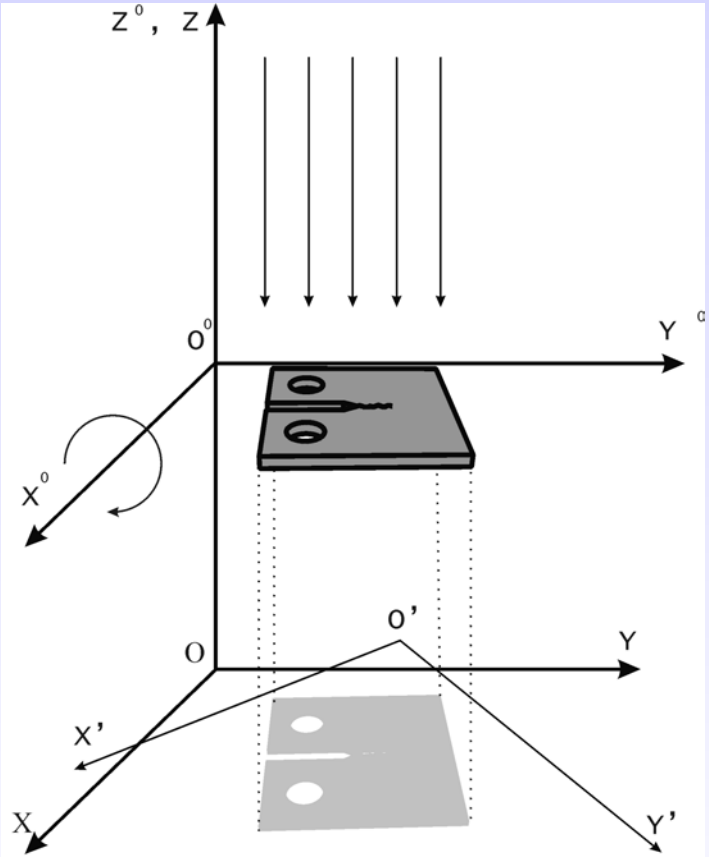


(X'O'Y') - detector coordinate system

($X^oY^oZ^o$) - sample coordinate system

# Projection geometry

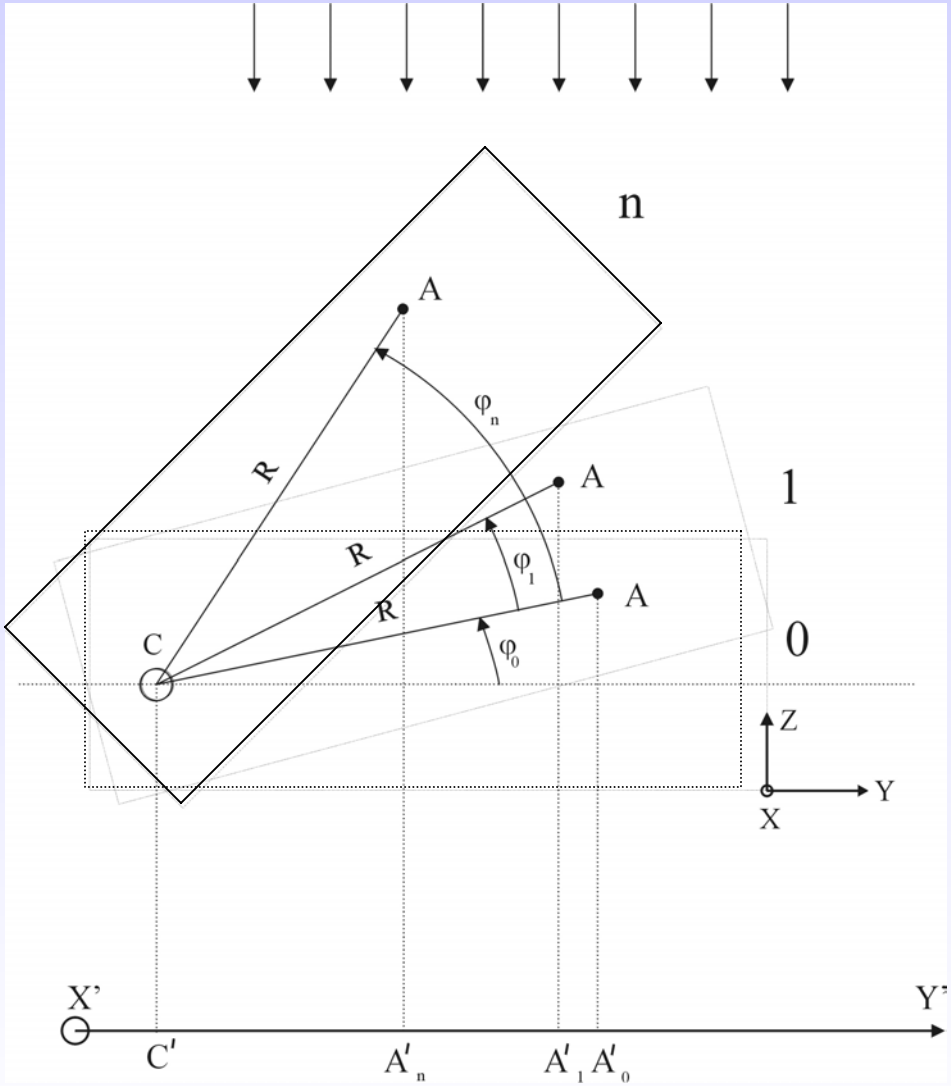


(X'Y') – detector coordinate system

(XYZ) – sample coordinate system

( C ) – Rotation axis

R– distance between the axis of rotation and the feature of interest A.

$A_x$, $A_y$ can be directly measured from the projection of A on the detector

$$\begin{cases} R = \dfrac{[C'A'_1]}{\cos(\varphi_0+\varphi_1)} \\ R = \dfrac{[C'A'_2]}{\cos(\varphi_0+\varphi_2)} \\ \cdots \\ R = \dfrac{[C'A'_n]}{\cos(\varphi_0+\varphi_n)} \end{cases}$$

$\varphi_0$ and R are unknown.

# **Projection geometry** (cont.)

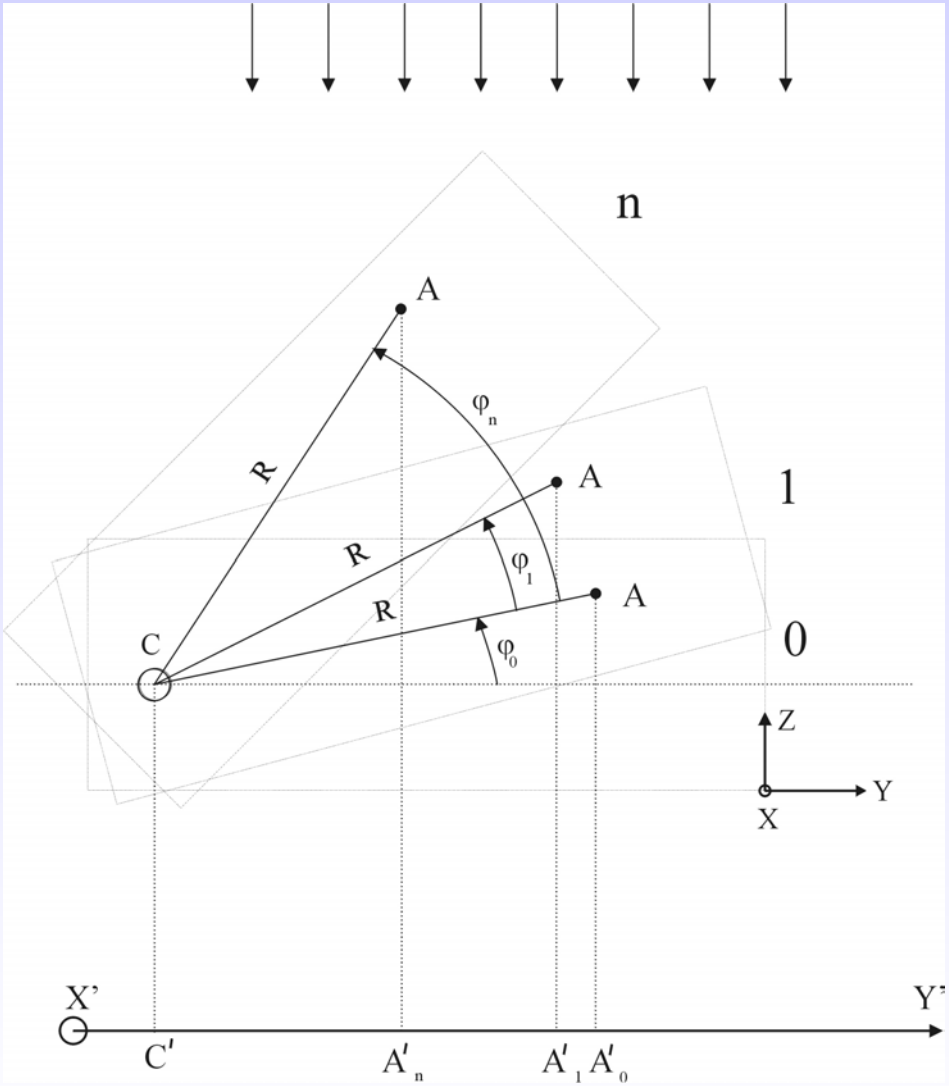


By measuring φ and A' for each projection, it is possible to reconstruct 3-D position of the feature A using more than two projections.

This increases accuracy by reducing random error component.

# Stereometry reconstruction

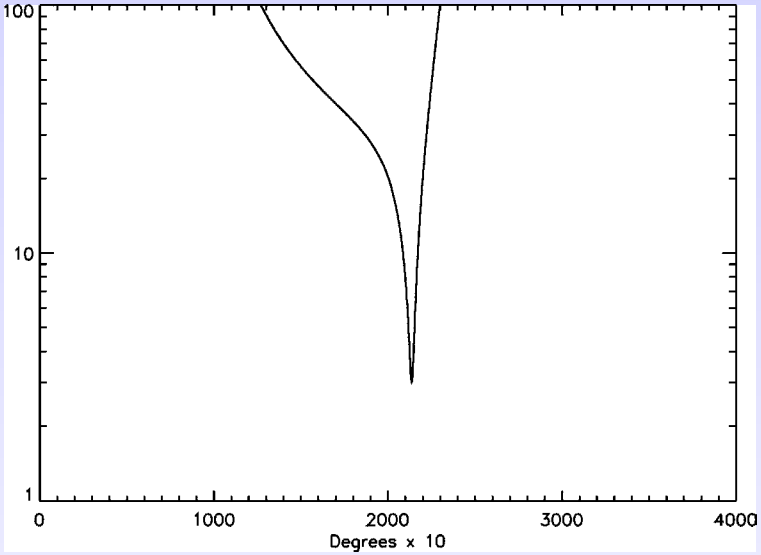


Typical plot of standard deviation of R vs. initial angle $\varphi_0$ for 10 projections.

# Compact tension sample geometry

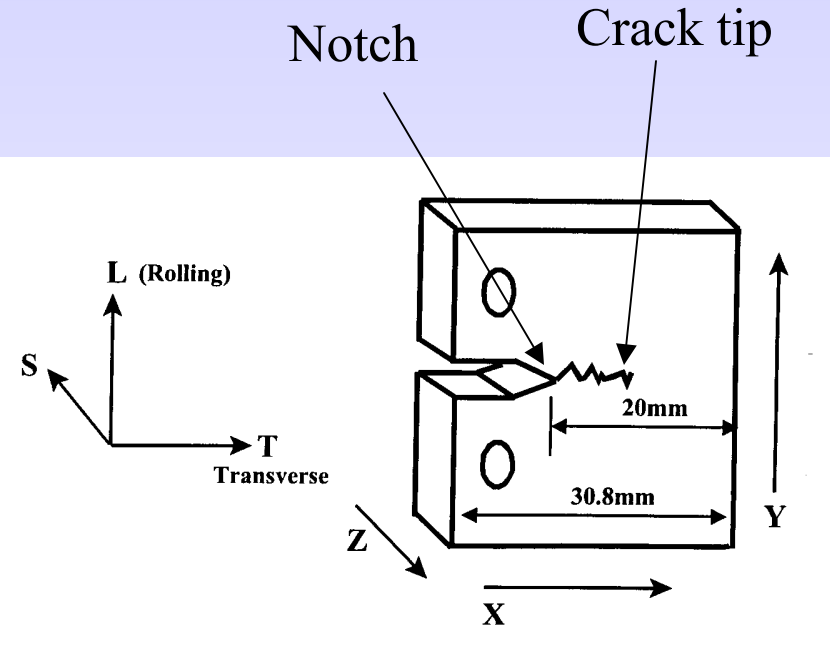


Cut from 12.7mm thick plate of AA 2090 T8E41 alloy.

Samples were scaled and machined according to ASTM standard E399-83

Thickness: 2.7 mm

Length: 31.8 mm

Width: 30.5 mm

# Experimental setup for phase contrast measurements at the beamline 1-ID-C (APS)

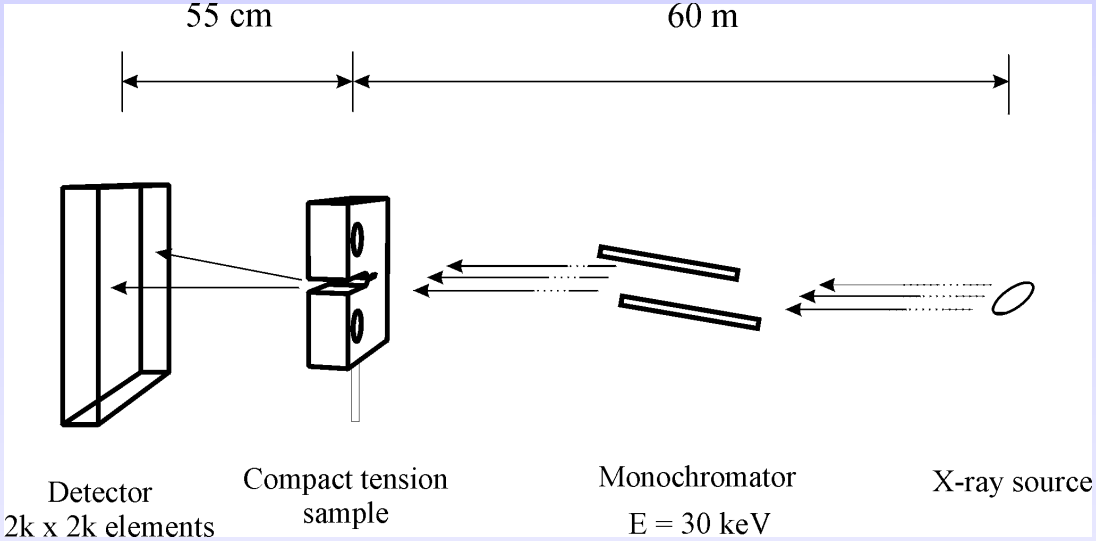


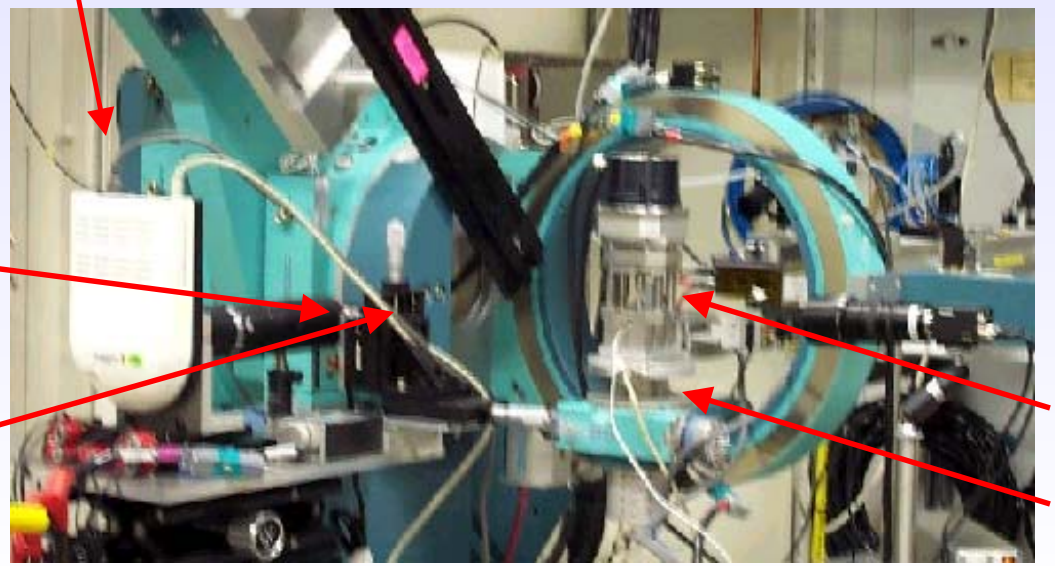

Magnifying objective

Scintillator crystal

Loading stage

Translation / Rotation stage

# X-ray phase contrast radiographs at different sample orientations

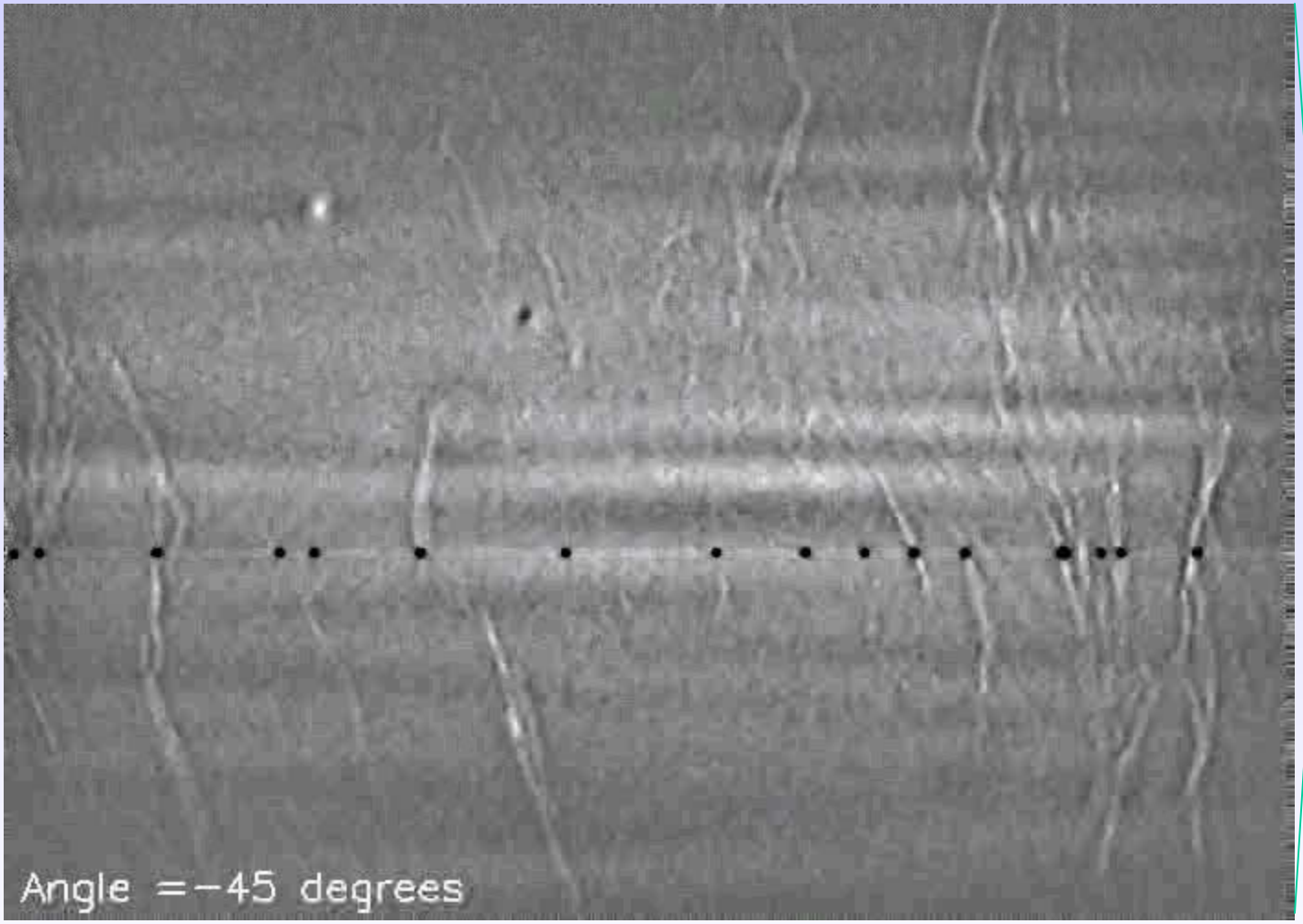


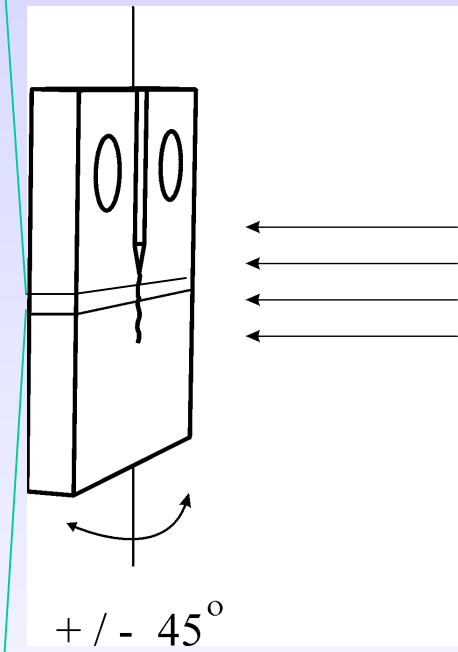

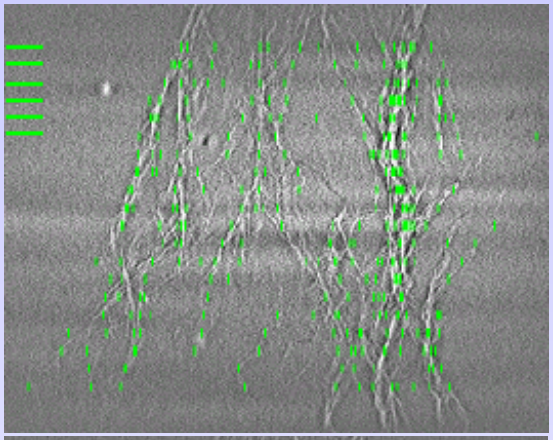

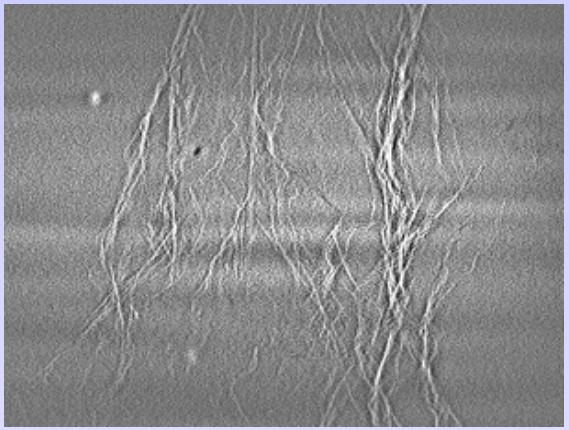

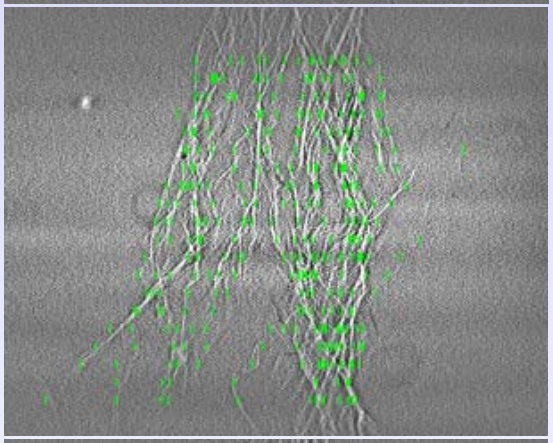

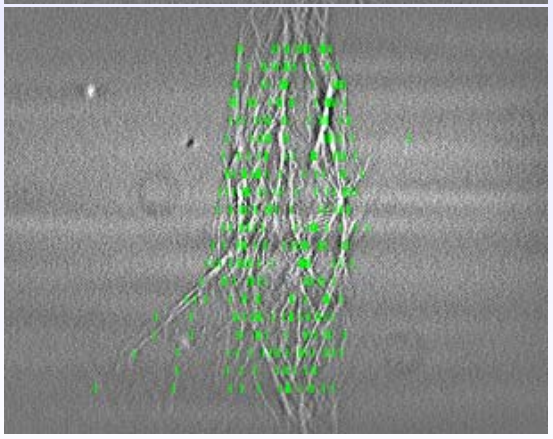

Phase contrast images of the crack taken at the angular interval of 10 degrees at the area 2mm from the notch. Rotation axis is coincident with the sample T direction and is vertical in the plane of the page.

Green marks on the left figures show positions of selected crack features. Figure on the right shows unmarked projection.

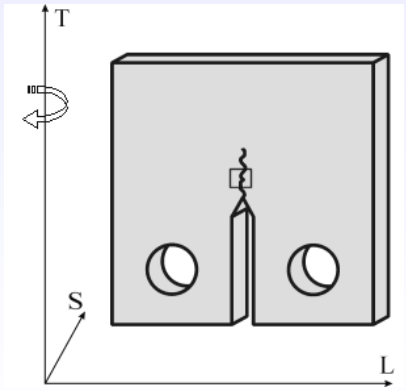


Vertical distance between two adjacent markers is 60μm

Profiles of the crack surface (parallel to the sample YZ plane) obtained with different methods at different distances from the notch.

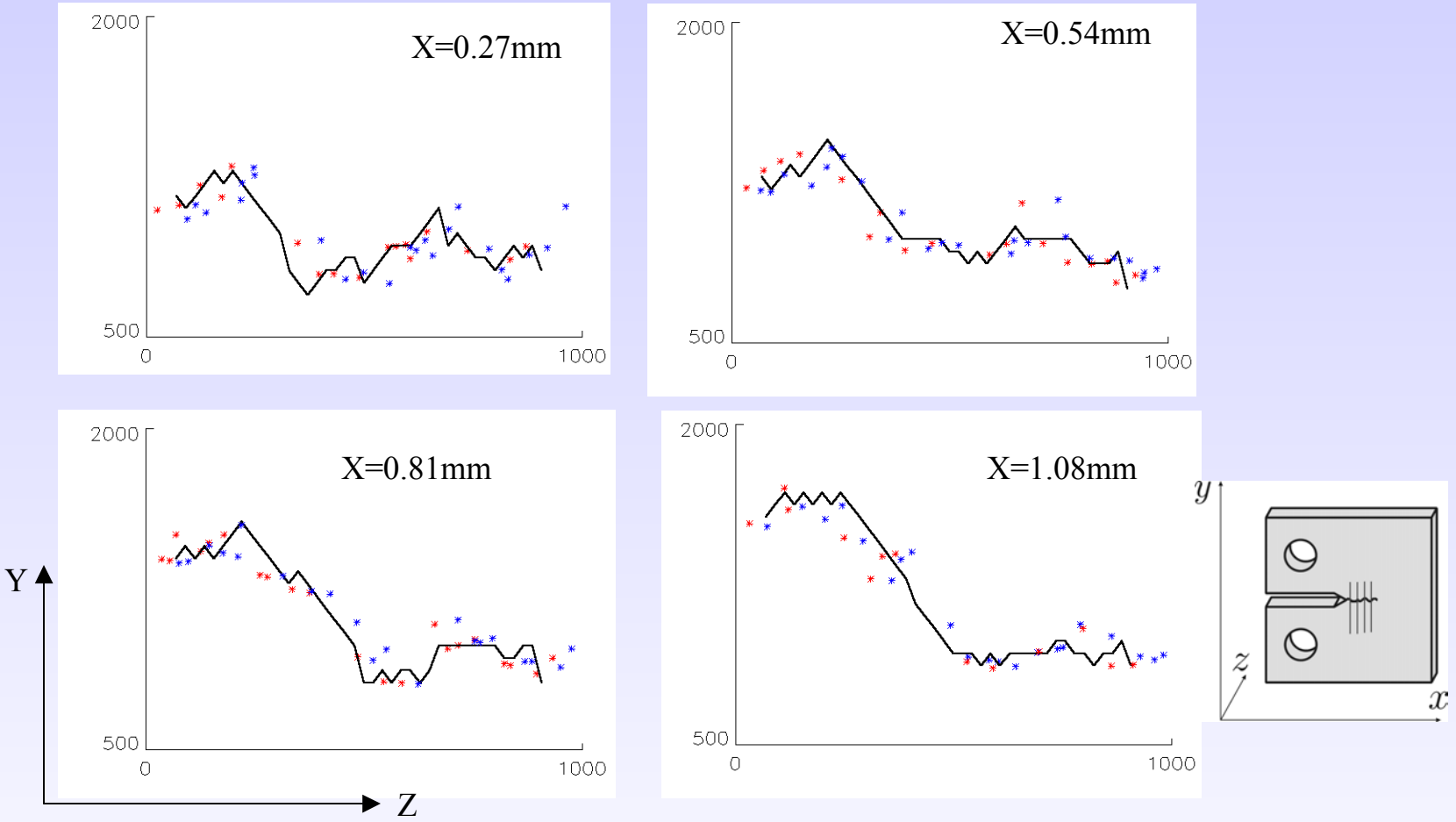


Red dots - stereometry with two phase projections, blue dots – stereometry with ten phase projections, Solid black line – microtomography. All units are μm.

# Crack surface from the phase contrast data

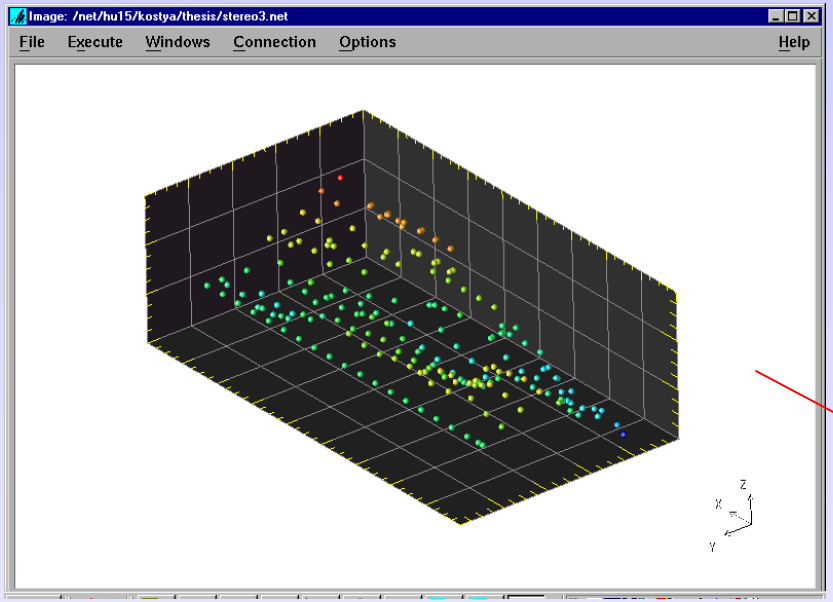


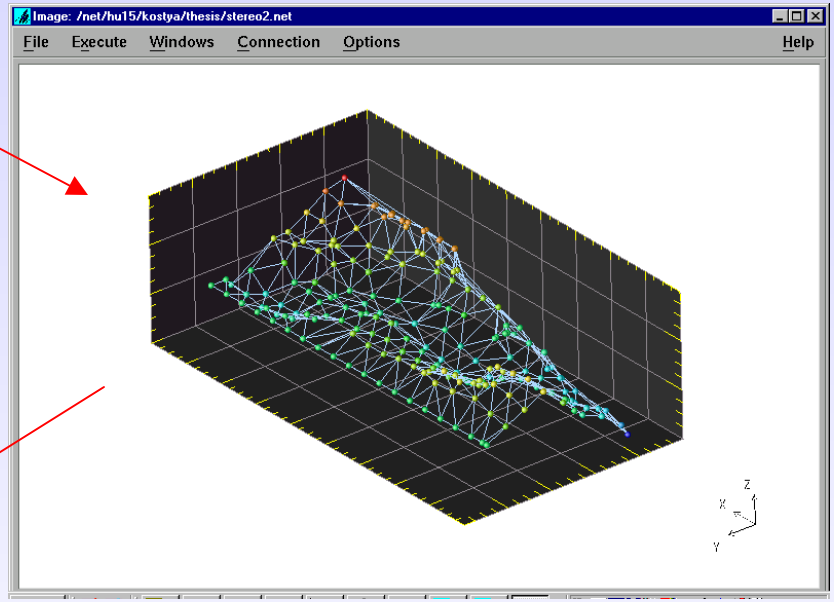


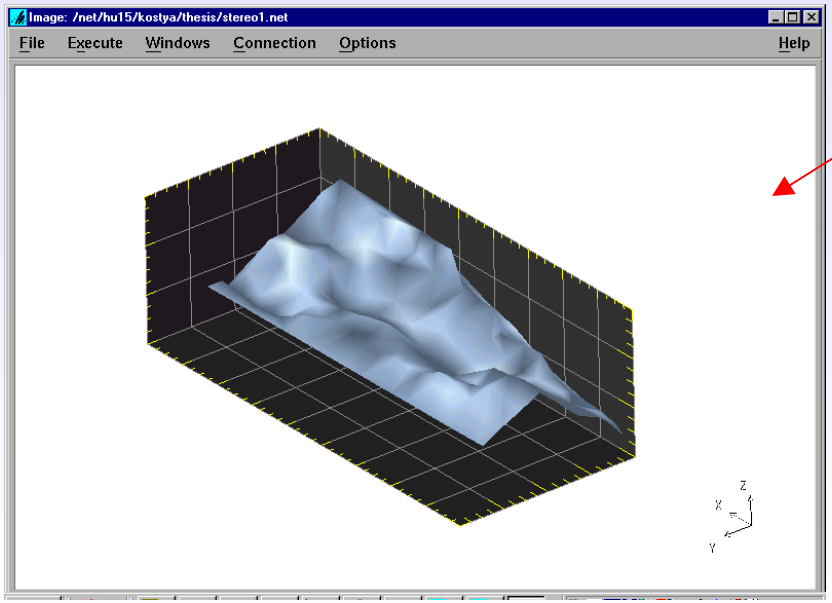

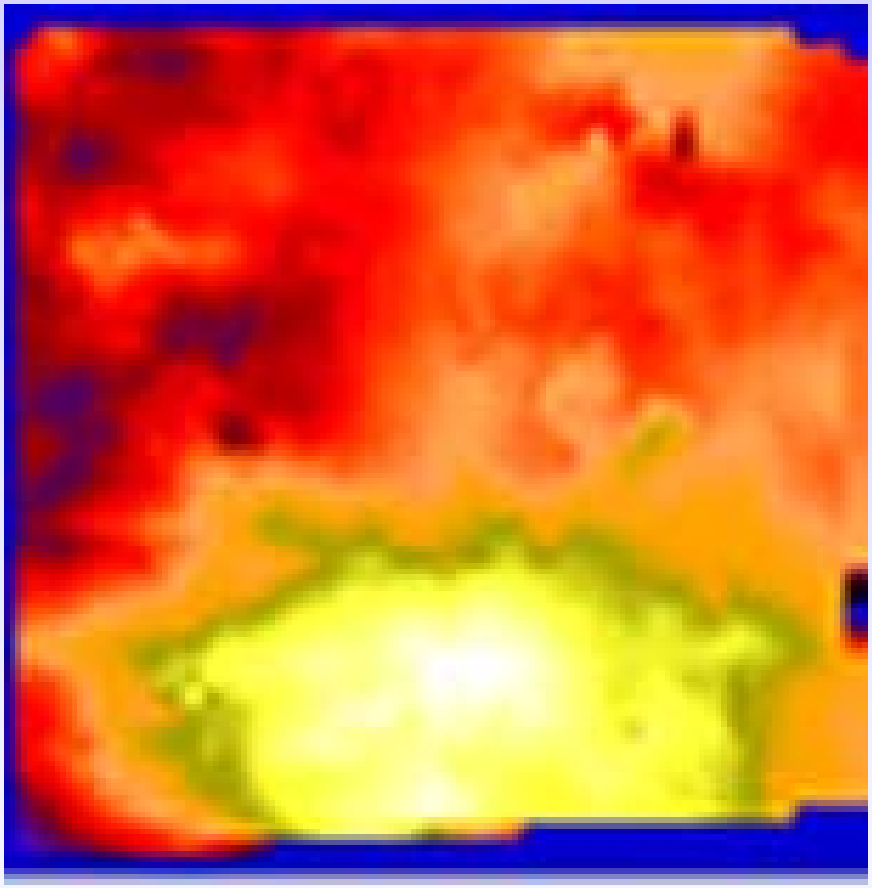

Crack surface map obtained from phase contrast stereometry with 1280 nodes

Horizontal field of view - 3.5mm

Z

X

Surface height (y)

0 3.9mm

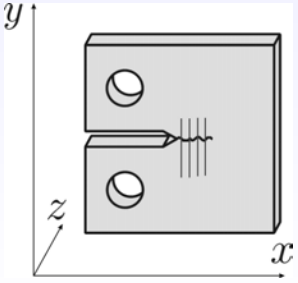

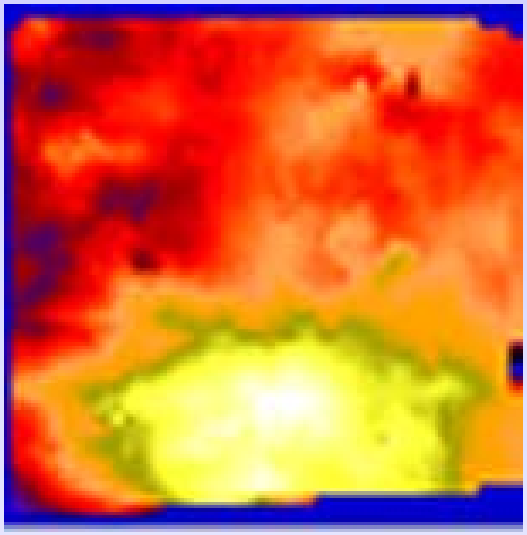


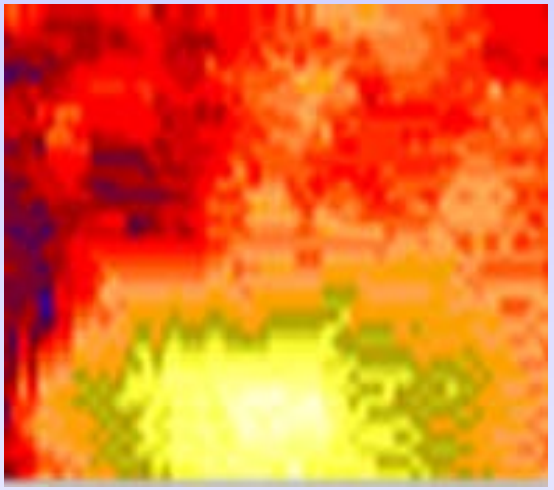

Surface height (y)

0 3.9mm

Crack surface map obtained from phase contrast stereometry with 1280 nodes

Crack surface map obtained with microtomography

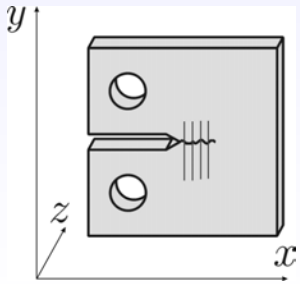

**Microtomography** **Phase contrast**

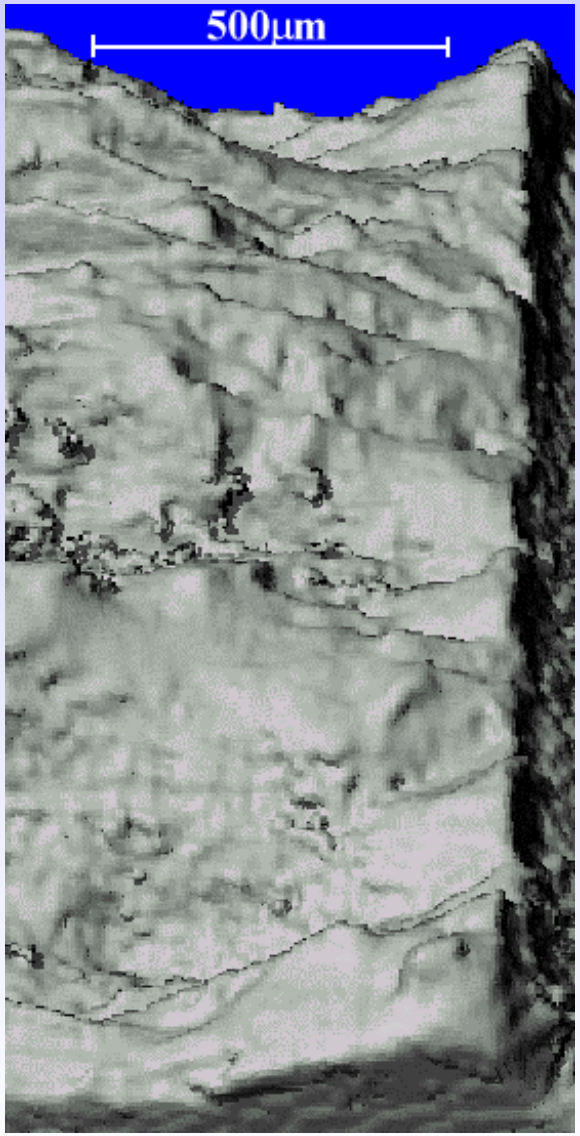


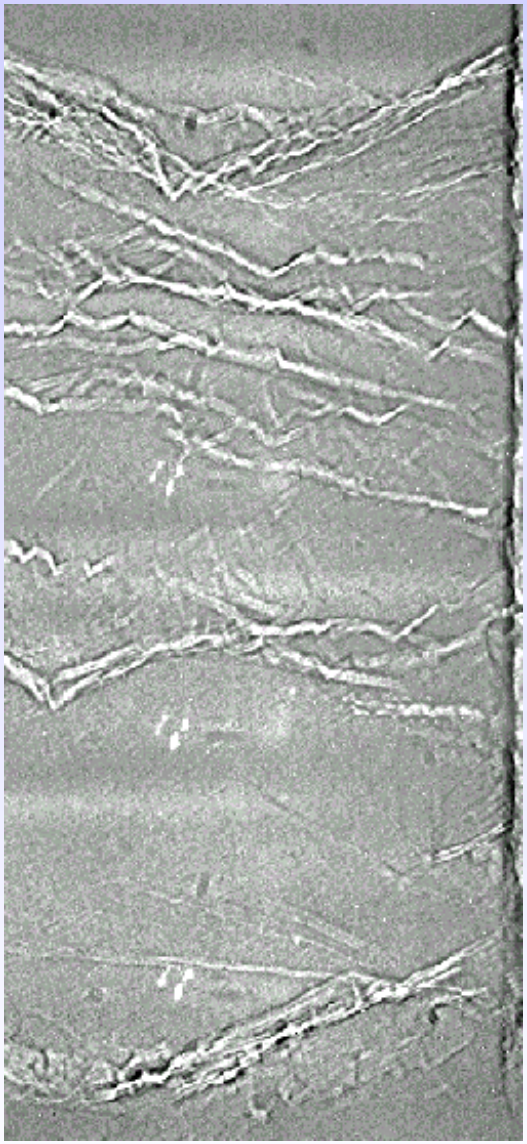

**Crack growth direction**

*On the right*: phase contrast radiograph of the fatigue crack in compact tension specimen CT-33M in the area near the notch

*On the left*: 3-D rendering obtained from microtomography data of the same area after the sample was broken and the volume of material near the notch was cut out

## Microtomography

## Phase contrast

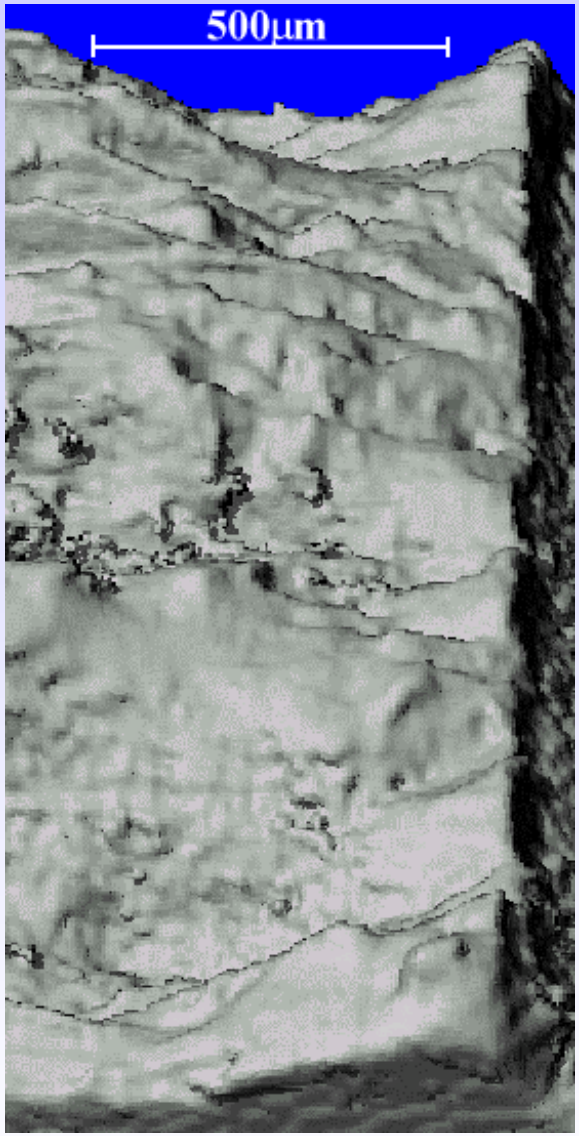


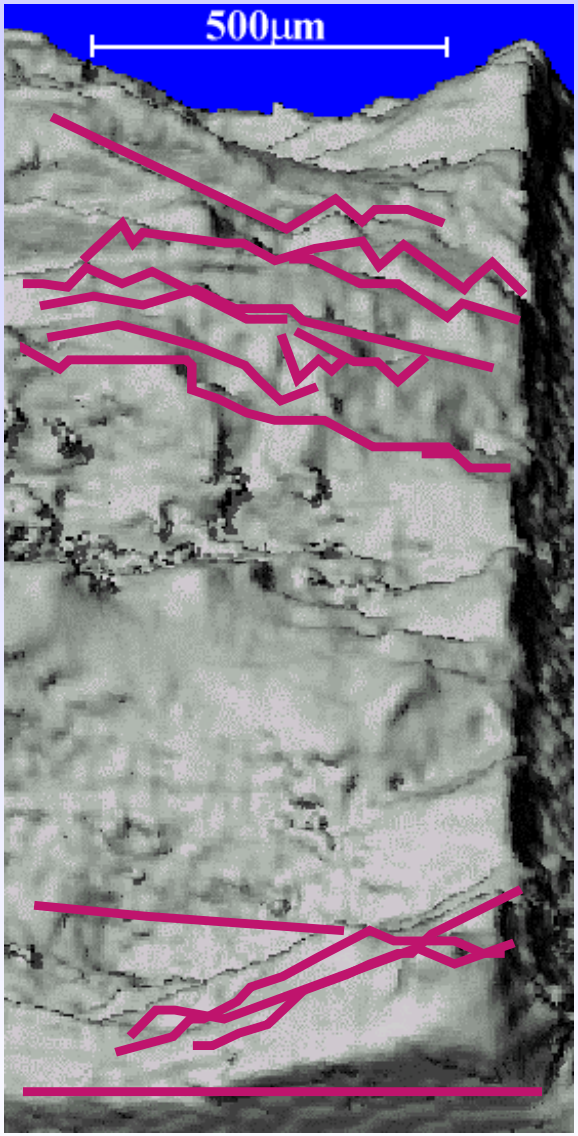


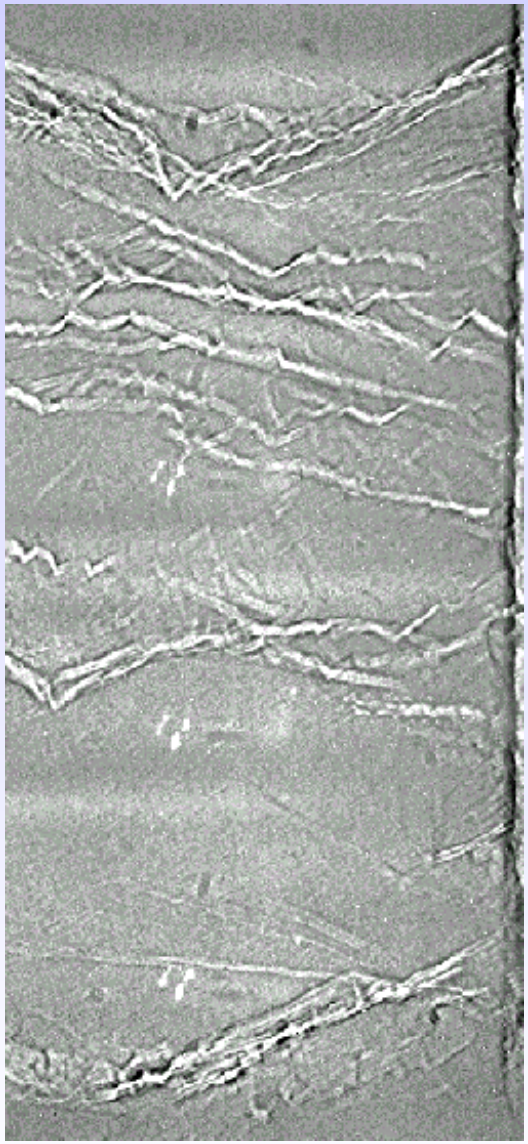

Crack growth direction

# Phase contrast experiment setup – Beamline 1-ID – Sample view

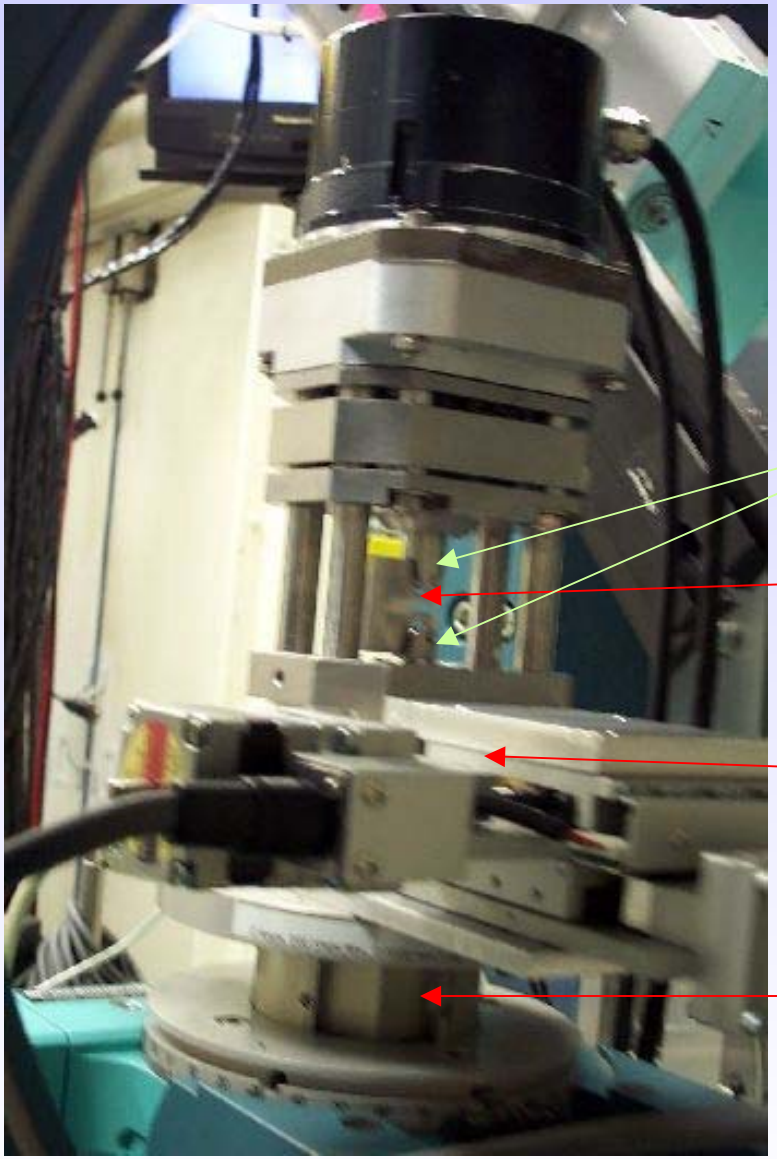

# Phase contrast images of crack opening with load

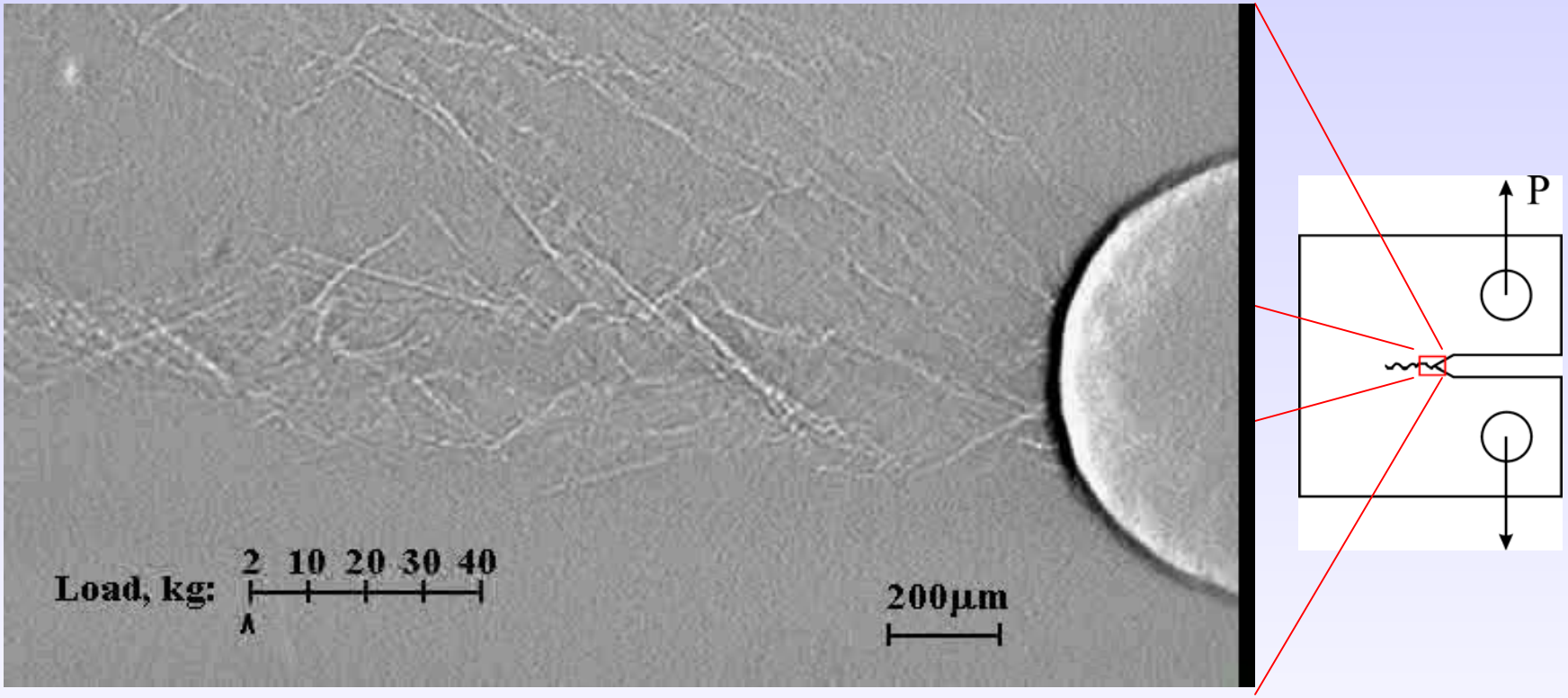

# Crack opening at different loads obtained from phase contrast and microtomography

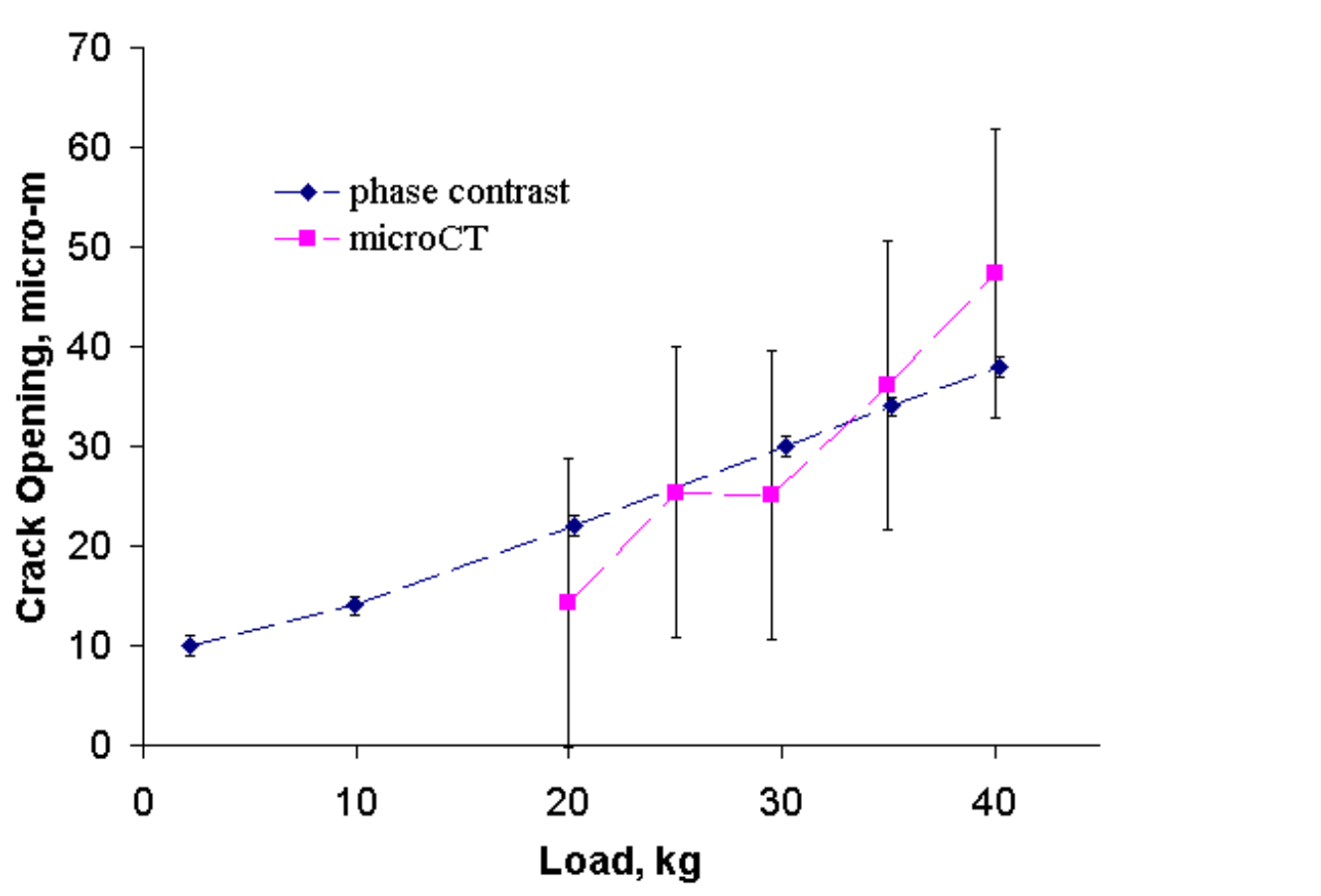

# Crack opening at different positions of the crack surface

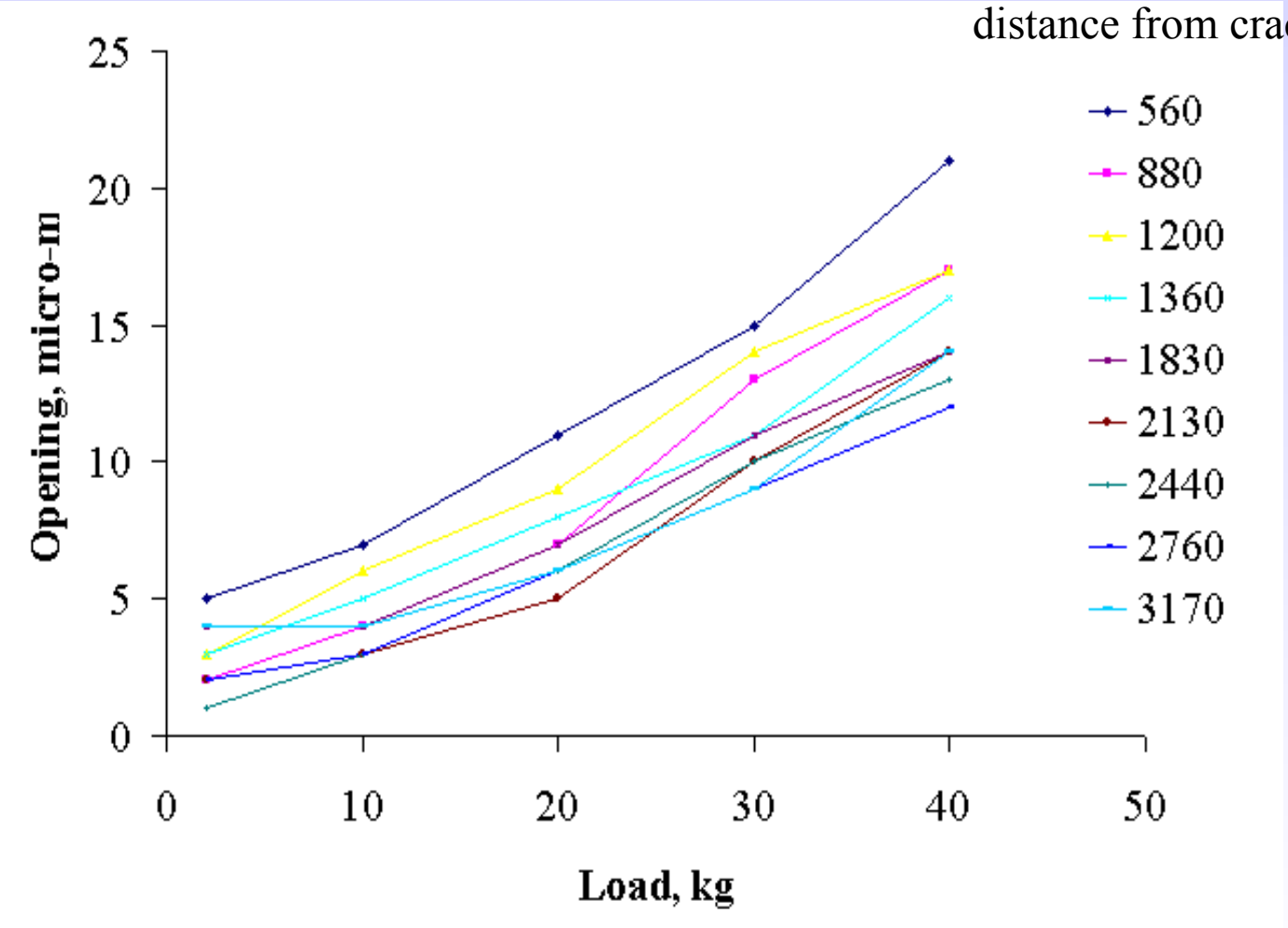

# Opening at 20kg and 40 kg along crack growth direction

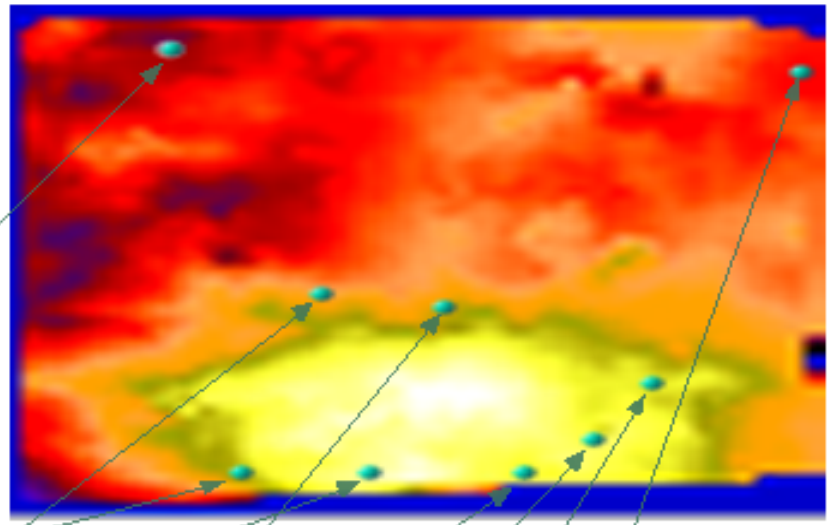

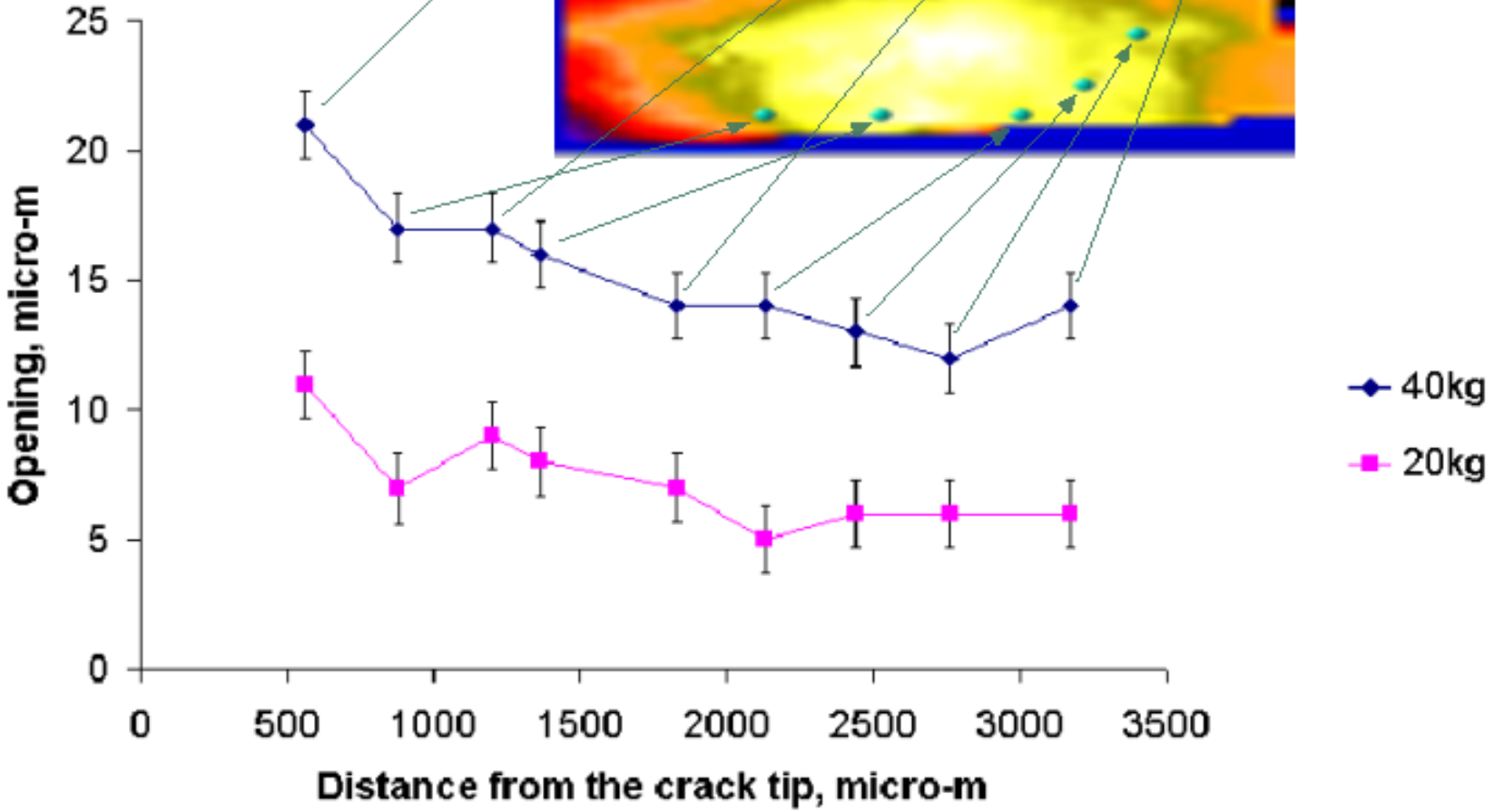

# Conclusion

- X-ray phase contrast imaging coupled with stereo reconstruction can be succesfully used to determine crack surface and position dependent opening of fatigue crack

- Can get higher resolution and sensitivity then with tomography methods

- Same approach to can be used for other plate-like samples containing a sharply defined object or series of objects

# Acknowledgments

• Experiments were conducted at Beamline 1-ID of the Advanced Photon Source, Argonne, IL. Wah-Keat Lee and Kamal Fezzaa (Argonne National Laboratory) helped with experiment setup and data collection

• This research is partially supported by the Office of Naval Research through grants N00014-89-J-1708 and N00014-94-1-0306

# X-RAY PHASE CONTRAST AND MULTIPLE - ANGLE STEREOMETRY FOR 3-D RECONSTRUCTION: FATIGUE CRACKS IN ALUMINUM

---

Konstantin Ignatiev

*Materials Science and Engineering Dept.*

*Georgia Institute of Technology*

Georgia Institute of Technology